Remote Sensing of Environment 154 (2014) 253–271

Contents lists available at ScienceDirect

Remote Sensing of Environment

journal homepage: www.elsevier.com/locate/rse

Parameterization of an ecosystem light-use-efficiency model for predicting savanna GPP using MODIS EVI

Xuanlong Ma [a,b,c], Alfredo Huete [b,*], Qiang Yu [b], Natalia Restrepo-Coupe [b], Jason Beringer [d], Lindsay B. Hutley [e], Kasturi Devi Kanniah [f], James Cleverly [b,g], Derek Eamus [b,g,h]

[a] Key Laboratory of Water Cycle and Related Land Surface Processes, Institute of Geographic Sciences and Natural Resources Research, Chinese Academy of Sciences, Beijing, 100101, China
[b] Plant Functional Biology and Climate Change Cluster (C3), University of Technology, Sydney, NSW, 2007, Australia
[c] University of Chinese Academy of Sciences, Beijing, 100049, China
[d] School of Geography and Environmental Science, Monash University, Melbourne, Victoria, 3800, Australia
[e] Research Institute for the Environment and Livelihoods, Charles Darwin University, Casuarina, Northern Territory, 0909, Australia
[f] Department of Geoinformation, Faculty of Geoinformation and Real Estate, Universiti Teknologi Malaysia, Skudai, Johor, 81310, Malaysia
[g] Australian Supersite Network, Terrestrial Ecosystem Research Network, University of Technology, Sydney, NSW, 2007, Australia
[h] National Centre for Groundwater Research and Training, University of Technology, Sydney, NSW, 2007, Australia

ARTICLE INFO

Article history:
Received 30 March 2014
Received in revised form 13 August 2014
Accepted 14 August 2014
Available online xxxx

Keywords:
Remote Sensing
Ecosystem Function
Carbon Cycle
Photosynthesis
Phenology
Gross Primary Production

ABSTRACT

Accurate estimation of carbon fluxes across space and time is of great importance for quantifying global carbon balances. Current production efficiency models for calculation of gross primary production (GPP) depend on estimates of light-use-efficiency (LUE) obtained from look-up tables based on biome type and coarse-resolution meteorological inputs that can introduce uncertainties. Plant function is especially difficult to parameterize in the savanna biome due to the presence of varying mixtures of multiple plant functional types (PFTs) with distinct phenologies and responses to environmental factors. The objective of this study was to find a simple and robust method to accurately up-scale savanna GPP from local, eddy covariance (EC) flux tower GPP measures to regional scales utilizing entirely remote sensing oservations. Here we assessed seasonal patterns of Moderate Resolution Imaging Spectroradiometer (MODIS) vegetation products with seasonal EC tower GPP (GPP_{EC}) at four sites along an ecological rainfall gradient (the North Australian Tropical Transect, NATT) encompassing tropical wet to dry savannas.

The enhanced vegetation index (EVI) tracked the seasonal variations of GPP_{EC} well at both site- and cross-site levels ($R^2 = 0.84$). The EVI relationship with GPP_{EC} was further strengthened through coupling with ecosystem light-use-efficiency (eLUE), defined as the ratio of GPP to photosynthetically active radiation (PAR). Two savanna landscape eLUE models, driven by top-of-canopy incident PAR (PAR_{TOC}) or top-of-atmosphere incident PAR (PAR_{TOA}) were parameterized and investigated. GPP predicted using the eLUE models correlated well with GPP_{EC}, with R^2 of 0.85 (RMSE = 0.76 g C m^{-2} d^{-1}) and 0.88 (RMSE = 0.70 g C m^{-2} d^{-1}) for PAR_{TOC} and PAR_{TOA}, respectively, and were significantly improved compared to the MOD17 GPP product ($R^2 = 0.58$, RMSE = 1.43 g C m^{-2} d^{-1}). The eLUE model also minimized the seasonal hysteresis observed between green-up and brown-down in GPP_{EC} and MODIS satellite product relationships, resulting in a consistent estimation of GPP across phenophases. The eLUE model effectively integrated the effects of variations in canopy photosynthetic capacity and environmental stress on photosynthesis, thus simplifying the up-scaling of carbon fluxes from tower to regional scale. The results from this study demonstrated that region-wide savanna GPP can be accurately estimated entirely with remote sensing observations without dependency on coarse-resolution ground meteorology or estimation of light-use-efficiency parameters.

1. Introduction

Measurement of landscape carbon fluxes is essential in global change studies (Baldocchi et al., 2001) but remains a challenge in the field, resulting in a scarcity of measurements available to validate and assess uncertainties in models and satellite products. By observing broad-scale patterns of ecosystem functioning, remote sensing can complement the restricted coverage afforded by eddy covariance (EC) measurements of gross primary production (GPP). Remote sensing estimates of GPP primarily utilize two technical approaches: (1) process models based on the light-use-efficiency (LUE) concept (Running et al., 2004; Xiao, Zhang, Hollinger, Aber, & Moore, 2005), and (2) empirical models

* Corresponding author at: Plant Functional Biology and Climate Change Cluster, University of Technology, Sydney, Broadway, NSW, 2007, Australia. Tel.: +61 2 9514 4084.
E-mail address: alfredo.huete@uts.edu.au (A. Huete).

http://dx.doi.org/10.1016/j.rse.2014.08.025
0034-4257/

based on relationships between flux tower estimates of GPP and satellite spectral vegetation indices (VIs) (Gitelson et al., 2006; Huete et al., 2006; Rahman, Sims, Cordove, & El-Marsri, 2005; Sims et al., 2008).

The LUE concept was first proposed by Monteith (1972) to estimate GPP by defining the amount of carbon fixed through photosynthesis as proportional to the solar energy absorbed by the plant. LUE is the energy conversion coefficient that can be defined as either the ratio of GPP to incident photosynthetic active radiation (PAR) or absorbed photosynthetic active radiation (APAR) (Gower et al., 1999), with APAR as the product of PAR and the fraction of absorbed photosynthetically-active radiation (fAPAR) (Monteith, 1972; Running et al., 2004). LUE models defined from APAR have been widely adopted to estimate GPP globally with the use of fAPAR and LUE (ε) (Monteith, 1972):

$$GPP = \varepsilon \times fAPAR \times PAR \tag{1}$$

The MODIS GPP product (MOD17) is based on the LUE concept and provides the first operational and near-real-time calculation of global GPP (Running et al., 2004; Zhao, Heinsch, Nemani, & Running, 2005). The MOD17 algorithm for calculating daily GPP is expressed as (Running et al., 2004):

$$GPP = \varepsilon_{max} \times 0.45 \times SW_{rad} \times fAPAR \times f(VPD) \times f(T_{min}) \tag{2}$$

where ε_{max} is the maximal light-use-efficiency, which is biome specific and obtained from a look-up table; SW_{rad} is short-wave downward solar radiation, of which 45% is assumed to be PAR; $f(VPD)$ and $f(T_{min})$ are the reduction scalars for water stress and low temperature, respectively (Running et al., 2004).

A major limitation of current LUE-based production efficiency models is that there are no direct measurements of LUE available at landscape scales. LUE is very difficult to parameterize since it varies significantly among vegetation types (Kergoat, Lafont, Arneth, Le Dantec, & Saugier, 2008; Turner et al., 2003), across seasons and phenophases (Jenkins et al., 2007; Sims et al., 2006), and under different types of environmental stress (Ruimy, Jarvis, Baldocchi, & Saugier, 1995). Consequently, maximal LUE values have to be specified for a limited number of biome types and then down-regulated by environmental stress scalars derived from coarse resolution, interpolated meteorological inputs (Heinsch et al., 2006; Zhao et al., 2005), which contribute uncertainties in output GPP (Heinsch et al., 2006; Sjöström et al., 2013; Yuan et al., 2010). Some studies reported that LUE models, when properly parameterized with site-level meteorological measurements, can provide good estimates of flux tower derived GPP (Kanniah, Beringer, Hutley, Tapper, & Zhu, 2009; Turner et al., 2003), while other studies found only moderately accurate estimates (Sjöström et al., 2013).

The MODIS GPP product has limited accuracy in estimating GPP of savannas (Jin et al., 2013; Kanniah et al., 2009; Sjöström et al., 2013), which are defined as woodland communities with a conspicuous perennial or annual graminoid substrata, with varying proportions of trees, shrubs and graminoids that form a structural continuum (Walker & Gillison, 1982). Across African savanna flux tower sites, Sjöström et al. (2013) reported MODIS GPP to underestimate tower-GPP over dry sites in the Sahel region due to uncertainties in the meteorological drivers and fAPAR data and underestimation of ε_{max}. At a woodland savanna site in Botswana, Jin et al. (2013) reported the MODIS GPP product to be substantially lower than tower-GPP during the green-up phase and higher than tower-GPP during the brown-down phase.

Kanniah et al. (2009) confirmed the usefulness of the MODIS GPP product for studying carbon dynamics at a northern Australian savanna site, yet important limitations were found due to the lack of representation of soil moisture in the MODIS GPP algorithm. These validation efforts of MOD17 GPP product at African and Australian savannas suggest a need to consider the limitations of current LUE based methodologies to estimate savanna GPP (Kanniah et al., 2009; Sjöström et al., 2013). Although it may be possible to improve the MODIS GPP product across global savannas by incorporation of a soil moisture term and using better quality meteorological data, it is also worthwhile to consider alternative methods for accurate and consistent remote sensing estimation of global GPP without dependency on numerous inputs (Sims et al., 2008).

Glenn, Huete, Nagler, and Nelson (2008) suggested that remote sensing is more suitable as a scaling tool when ground data are available, rather than for solving complicated physical models. Remote sensing can greatly simplify the up-scaling of ecosystem processes, such as photosynthesis and evapotranspiration, from an expansive network of flux towers to larger landscape units and to regional or even global scales (Glenn et al., 2008). As top-of-canopy measurements, flux towers do not require knowledge of LAI or details of canopy architecture to estimate fluxes (Baldocchi et al., 2001; Glenn et al., 2008). Meanwhile, the measurement footprint of flux towers partially overlaps the pixel size of daily-return satellites (e.g., 250 m for MODIS). With the fast evolving regional and global flux networks (e.g., FLUXNET, AmeriFlux, AsiaFlux, and OzFlux) and ongoing space-borne sensors (e.g., MODIS, MERIS, and VIIRS), enormous opportunities now exist to develop more robust and consistent methods for scaling of carbon fluxes across biomes, seasons, and extreme dry to wet years through better coupling of these two independent sources of observations (Huete et al., 2008).

The spatial extension of tower measured carbon fluxes using satellite spectral VIs have been investigated across a wide range of natural and agricultural ecosystems. For example, Wylie et al. (2003) reported a strong relationship between NDVI and daytime CO_2 flux in a sagebrush-steppe. Over North America, Rahman et al. (2005) found that EVI can provide reasonably accurate estimates of GPP Sims et al. (2006) further concluded EVI relationships with tower-GPP to be better than that with MOD17 GPP when data from winter periods of inactive photosynthesis were excluded. In Amazonia, Huete et al. (2006) observed a consistent linear relationship between MODIS EVI and tower GPP in both primary forest and converted pasture such that MODIS EVI did not saturate over the high foliage densities of tropical rainforests. Huete et al. (2008) further extended this study to three distinct Monsoon Asia tropical forest sites and found similar linear relationships between EVI and tower GPP, potentially offering opportunities for region-wide extension of carbon fluxes across the heterogeneous canopies of Southeast Asia. Over Scandinavian forest sites, Olofsson et al. (2008) reported strong correlations between EVI and GPP, while NDVI exhibited saturation in areas with high foliage density. Across African savannas, Sjöström et al. (2011) found EVI to track the seasonal dynamics of tower GPP more closely than MOD17 GPP. More recently, Ma et al. (2013) observed good convergence between MODIS EVI and tower GPP across north Australian mesic and xeric savannas, confirming the potential to link these two independent sources of observations for better understanding of savanna carbon dynamics.

Other studies have investigated coupling EVI with satellite retrieved land surface variables for improved predictions of tower derived GPP. For example, Sims et al. (2008) used a Temperature and Greenness (T-G) model, based on EVI and land surface temperature (LST), and substantially improved the correlation between predicted and tower derived GPP across North America compared with MOD17 GPP or EVI alone. Gitelson et al. (2006) found that a Greenness and Radiation (G-R) model, coupling canopy chlorophyll content with PAR, provided a more robust estimation of crop GPP. Peng, Gitelson, and Sakamoto (2013) applied the G-R model to estimate GPP using chlorophyll-related VIs (VI_{chl}), such as NDVI, EVI, and the wide dynamic range vegetation index (WDRVI), and found high accuracies in GPP estimations over irrigated and rain fed croplands. Wu et al. (2009) also found a tight relationship between canopy total chlorophyll content and GPP/PAR, thereby providing new ways to estimate GPP from chlorophyll-related spectral indices.

From a resource-use-efficiency perspective, the coupling of VI_{chl} and PAR for the estimation of GPP implies that VI_{chl} is essentially a measure of LUE defined and based on PAR. To distinguish the LUE (ε) based on

APAR from LUE based on PAR, we define the former as ε (i.e., GPP/APAR) and the latter as ecosystem light-use-efficiency (eLUE). eLUE can be computed and modelled as:

$$\mathrm{eLUE} = \frac{\mathrm{GPP}}{\mathrm{PAR}} = \mathrm{fAPAR} \times \varepsilon = f(\mathrm{VI_{chl}}) \tag{3}$$

where $f(\mathrm{VI_{chl}})$ can be calibrated by regression with flux tower derived eLUE against $\mathrm{VI_{chl}}$. eLUE (GPP/PAR) differs from ε (GPP/APAR) in that it combines the biological drivers of photosynthesis (fAPAR) with net photosynthetic efficiency (ε) resulting from environmental stress and leaf age phenology. The benefit of using eLUE in up-scaling of GPP is that eLUE does not require partitioning of plant functioning into both fAPAR and ε terms, thus simplifying remote sensing based estimates of vegetation productivity. This reduces associated scaling uncertainties introduced by coarse resolution meteorological inputs and the need to define biome specific ε_{max} values in mixed plant functional types (C_3 trees and C_4 grasses) savannas.

The objectives of this study were (1) to assess seasonal synchronies and performances of various satellite vegetation products and models for tracking seasonal variations in $\mathrm{GPP_{EC}}$ along an ecological rainfall gradient encompassing northern Australia mesic to xeric savannas; (2) to examine the use of ecosystem light-use-efficiency (eLUE) framework for up-scaling tower derived GPP to regional scales from entirely remote sensing observations; and (3) to assess scale issues for extrapolating tower GPP across biologic phenophases, including green-up and brown-down periods.

2. Methods

2.1. Study area

This study focused on a sub-continental scale ecological rainfall gradient of more than 1100 km, which is known as the North Australian Tropical Transect (NATT) (Koch, Vitousek, Steffen, & Walker, 1995) (Fig. 1). The NATT was conceptualized in the mid-1990s as part of the International Geosphere Biosphere Programme (IGBP) (Koch et al., 1995). Together with the Kalahari transect in southern Africa and the SALT (Savanne à Long Terme) transect in West Africa, these three transects have been used extensively in the study of global savannas (Walker, Steffen, Canadell, & Ingram, 1999).

Carbon flux measurements from four EC flux tower sites located along the NATT transect were used (Fig. 1 & Table 1), including three mesic Eucalypt woodland sites: Howard Springs, Adelaide Rivers, and Daly River (Beringer et al., 2011) and a xeric *Acacia* woodland site: Ti Tree (Cleverly et al., 2013; Eamus et al., 2013). These sites are part of OzFlux (Australian and New Zealand Flux Research and Monitoring Network) under TERN (Australian Terrestrial Ecosystem Research Network). These sites represent the two most common savanna classes present in Australia, namely *Eucalyptus* (and closely-related *Corymbia*) woodland and *Acacia* woodland.

2.2. Eddy covariance tower derived GPP (GPP_{EC})

The original Level 3 OzFlux data were pre-processed to ensure consistency among sites and reduce the uncertainties in computed fluxes, including general quality control assessment, removal of outliers, and correction for low turbulence periods. A second-order Fourier regression was fitted to nighttime net ecosystem exchange (NEE) time series, which is assumed to be representative of ecosystem respiration (R_{eco}), using the method proposed by Richardson and Hollinger (2005):

$$R_{eco} = f_0 + s_1 \times \sin(D_\pi) + c_1 \times \cos(D_\pi) + s_2 \times \sin(2 \times D_\pi) + c_2 \times \cos(2 \times D_\pi) + \varepsilon \tag{4}$$

where f_0, s_1, c_1, s_2 and c_2 are Fourier fitted coefficients, $D_\pi = DOY \times 360/365$ (DOY: Day of Year), and ε is the regression residuals. We used this method due to its minimal use of environmental covariates to compute R_{eco} (Richardson & Hollinger, 2005). GPP were then derived as $GPP = R_{\mathrm{eco}} - NEE$. As the intent of this study was to obtain a reliable time series of GPP observations to compare with satellite observations, we computed 8-day average GPP to match the temporal resolution of MODIS products.

2.3. Meteorological and soil moisture data

Half-hourly values of air temperature (T_a, °C), precipitation, shortwave incoming solar radiation (SW_{in}, W m^{-2}), and volumetric soil water content (SWC, %) measured at 10 cm depth were obtained from the flux tower sites. As with the fluxes, half-hourly measurements were then aggregated to 8-day for comparison with satellite observations.

2.4. Satellite data

2.4.1. MODIS surface reflectances and vegetation indices

Approximately 13.5 years (February 2000–July 2013) of 8-day 500 m Surface Reflectance product (MOD09A1, Collection 5, tiles h30v10 and h30v11) (Vermote, Saleous, N. Z., & Justice, 2002) were obtained through the online Data Pool at the NASA Land Processes Distributed Active Archive Centre (LP DAAC), USGS/Earth Resources Observation and Science (EROS) Centre, Sioux Falls, South Dakota (https://lpdaac.usgs.gov/data_access). A 3 × 3 MOD09A1 500 m pixel window (2.25 km^2) was used to extract reflectances time series to match the footprint of EC towers and to compute the vegetation indices. Within the extracted reflectance time series, we selected data satisfying all of the following conditions based on the 16-bit QC (500 m state flags) and 32-bit QC (500 m reflectance band quality) layers provided along with MOD09A1: (1) corrected product produced at ideal quality all bands; (2) highest quality for band 1–7; (3) atmospheric correction performed; (4) adjacency correction performed; (5) MOD35 cloud flag indicated "clear"; (6) no cloud-shadow was detected; (7) low or average aerosol quantities.

NDVI and EVI are widely used as proxies of canopy "greenness", an integrative composite property of green leaf area, green foliage cover, structure, and leaf chlorophyll content (Myneni & Williams, 1994). VIs are robust and seamless biophysical measures, computed identically across all pixels in time and space regardless of biome type, land cover condition, and soil type (Huete & Glenn, 2011). EVI was used as an optimized version of NDVI that effectively reduces soil background influences and atmospheric noise variations (Huete et al., 2002). The equations defining NDVI (Rouse et al., 1973) and EVI are:

$$\mathrm{NDVI} = \frac{\rho_{\mathrm{nir}} - \rho_{\mathrm{red}}}{\rho_{\mathrm{nir}} + \rho_{\mathrm{red}}}$$
$$\mathrm{EVI} = 2.5\frac{\rho_{\mathrm{nir}} - \rho_{\mathrm{red}}}{\rho_{\mathrm{nir}} + 6\rho_{\mathrm{red}} - 7.5\rho_{\mathrm{blue}} + 1} \tag{5}$$

where ρ_{nir}, ρ_{red} and ρ_{blue} are reflectances of the near infrared (841–876 nm), red (620–670 nm), and blue (459–479 nm) bands of the MODIS sensor, respectively. Hereafter we will refer NDVI and EVI derived from MOD09A1 reflectances specifically as $\mathrm{NDVI_{MOD09}}$ and $\mathrm{EVI_{MOD09}}$, respectively.

2.4.2. MODIS GPP product (GPP_{MOD17})

We used the global 1-km 8-day MODIS GPP product (MOD17A2, Collection 055, tiles h30v10 and h30v11) from January 2000 through December 2012 obtained from NASA LP DAAC and USGS EROS repository (https://lpdaac.usgs.gov/data_access) (Running et al., 2004). The algorithm calculates daily GPP as a function of incoming solar radiation, conversion coefficients, and environmental stresses (Running et al., 2004). We used a 1 km^2 window to extract MOD17A2 GPP time series

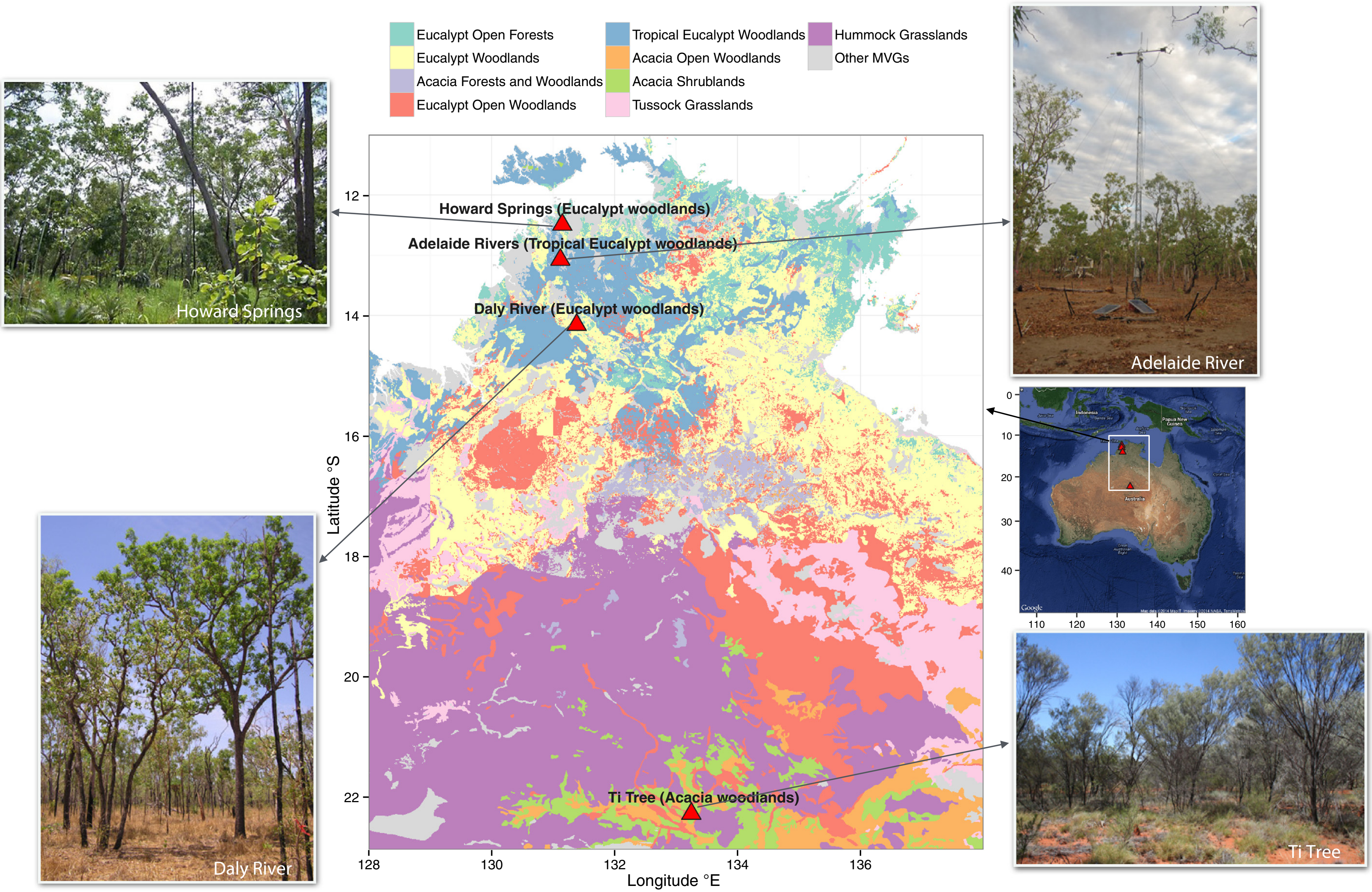

Fig. 1. Spatial extent of the NATT study area. The red triangles indicate the locations of the four EC flux tower sites. Background is the map of Australian Major Vegetation Groups (MVGs, v4.1), provided by Australian National Vegetation Information System (NVIS, 2007). Central-right small panel shows the locations of the study area over the Australian continent (image source: Google Earth). Photographs show the ground-view of each flux tower site (image source: www.OzFlux.org.au). Top-left: early wet season 2010 at Howard Springs; bottom-left: dry season at Daly River; top-right: Adelaide River flux tower; bottom-right: woodland floor and understorey at Ti Tree.

Table 1
Summary of EC flux tower sites in the NATT study area.

Site	Longitude (°E)	Latitude (°S)	Elevation (m)	Vegetation Type	Overstorey	Understorey	Canopy Height (m) [a]	Soil [a]	MAP ± σ (mm) [b]
Howard Springs	131.150	12.495	64	Eucalypt Woodlands	*Eucalyptus miniata, Erythrophleum chlorostachys, Terminalia ferdinandiana*	*Sorghum spp.*	18.9	red kandosol	1722 ± 341
Adelaide Rivers	131.118	13.077	90	Tropical Eucalypt Woodlands	*E. tectifica, Planchonia careya, Buchanania obovata*	*Sorghum spp.*	12.5	yellow hydrosol	1692 ± 373
Daly River	131.383	14.159	52	Eucalypt Woodlands	*T. grandiflora, E. tetrodonta, E. latifolia*	*Sorghum spp., Heteropogon triticeus*	16.4	red kandosol	1295 ± 334
Ti Tree	133.249	22.283	606	*Acacia* Woodlands	*C. opaca, E. victrix, Acacia aneura*	*Psydrax latifolia, Thyridolepsis michelliana, Eragrostis eriopoda, Eriachne pulchella*	6.5	red kandosol	443 ± 222

[a] Cited from OzFlux Web site: www.OzFlux.org.au
[b] MAP = mean annual precipitation, calculated using Australian Bureau of Meteorology gridded rainfall data for each site using data of 12 hydrological years (2000.07.01–2012.06.30) (Jones, Wang, & Fawcett, 2009). To calculate the annual rainfall, we used hydrological year defined from July 1 to following June 30, instead of calendar year.

for each flux tower. We used the QA layers embedded in the MOD17A2 product to select data satisfying all the following: (1) MODLAND_QC bits indicate good quality; (2) detectors apparently fine for up to 50% of channels 1, 2; (3) no significant clouds present (clear).

2.4.3. MODIS LAI/fAPAR products (LAI_{MOD15} and $fAPAR_{MOD15}$)

For comparison, we also obtained MODIS 8-day global 1-km LAI/fAPAR product (MOD15A2, Collection 5, tiles h30v10 and h30v11) from February 2000 to May 2013 (Myneni et al., 2002) through NASA LP DAAC and USGS EROS repository (https://lpdaac.usgs.gov/data_access). The main algorithm for retrieval of LAI/fAPAR is based on a biome specific lookup table (LUT), which is generated using a three-dimensional radiative transfer (RT) model or using vegetation indices when the main algorithm failed (Myneni et al., 2002). For each field site, a 1 km^2 window was applied to obtain the LAI_{MOD15} and $fAPAR_{MOD15}$ time series. Within the extracted time series, we selected the data satisfying all of the following conditions (1) main (RT) algorithm used, best results possible (no saturation); (2) significant clouds not present (clear); (3) no or low atmospheric aerosol.

2.4.4. MODIS LST product, daytime (LST_{MOD11})

We obtained 1-km 8-day MODIS global land surface temperature (LST) product (MOD11A2, Collection 5, tiles h30v10 and h30v11) from NASA LP DAAC and USGS EROS repository (https://lpdaac.usgs.gov/data_access). The MOD11 LST product was generated based on the generalized split-window algorithm (Wan & Dozier, 1996). At each flux tower site, we applied a 1 km^2 window to obtain the daytime LST_{MOD11} time series. We selected the LST_{MOD11} observations satisfying all the following conditions: (1) LST produced with good quality; (2) good data quality of L1B in 7 TIR (thermal infrared) bands; (3) average emissivity error ≤ 0.02; (4) average LST error ≤ 2 K.

2.5. Variations of EVI-based GPP models

We compared the performances of two variations of widely used EVI-based GPP models, namely the T-G (Temperature and Greenness) model (Sims et al., 2008) and G-R (Greenness and Radiation) model (Gitelson et al., 2006).

2.5.1. Temperature–Greenness model

The T-G model was formulated as (Sims et al., 2008):

$$GPP \propto EVI_{scaled} \times LST_{scaled} \tag{6}$$

where the EVI_{scaled} was calculated following Sims et al. (2008):

$$EVI_{scaled} = EVI - 0.1 \tag{7}$$

The LST_{scaled} can be computed as (Sims et al., 2008):

$$LST_{scaled} = \min[(LST/30); (2.5-(0.05 \times LST))] \tag{8}$$

LST_{scaled} sets GPP to zero when LST is less than zero and thus defines the inactive winter period (Sims et al., 2008). LST_{scaled} also accounts for low temperature limitations to photosynthesis when LST is between 0 and 30 °C, as well as accounts for high temperature and high VPD stress in sites that exceed LST values of 30 °C (Sims et al., 2008).

2.5.2. Greenness–Radiation model

The G-R model was formulated as (Gitelson et al., 2006; Peng et al., 2013):

$$GPP \propto VI_{chl} \times PAR_{TOC} \tag{9}$$

where VI_{chl} is the chlorophyll-related spectral index. We used EVI as VI_{chl} following Wu, Chen, and Huang (2011). PAR_{TOC} is the tower measured PAR incident at the top-of-canopy (MJ m^{-2} d^{-1}), computed as 50% of the tower measured shortwave incoming radiation (MJ m^{-2} d^{-1}) following Papaioannou et al. (1993).

PAR_{TOC} can be obtained at flux tower sites but not across the entire region. Therefore, in addition to the original G-R model driven by PAR_{TOC}, we also proposed a modified version by replacing PAR_{TOC} with PAR incident at the top-of-atmosphere (PAR_{TOA}) to extrapolate beyond the tower footprint. The modified G-R model was formulated as:

$$GPP \propto EVI \times PAR_{TOA} \tag{10}$$

where PAR_{TOA} (MJ m^{-2} d^{-1}) was computed as the 40% of top-of-atmosphere incoming solar radiation (R_{TOA}, MJ m^{-2} d^{-1}) following Monteith and Unsworth (2013). R_{TOA}, also known as extraterrestrial radiation, is the amount of global horizontal radiation that a location on Earth would receive if there was no atmosphere or clouds (i.e., in outer space). The R_{TOA} can be computed from Earth-Sun geometry:

$$R_{TOA} = \frac{S_0}{\pi}\left(\frac{r_0}{r}\right)^2 (H \sin\phi \sin\delta + \sin H \cos\phi \cos\delta) \tag{11}$$

where S_0 is solar constant (1366 W m^{-2} or 118.02 MJ m^2 d^{-1}); r is the Earth-Sun distance; r_0 is the mean Earth-Sun distance; H is sun hour angle at sunset;   is latitude (°); and δ is solar declination (°).

The PAR_{TOA} used in this study is essentially similar to potential PAR ($PAR_{potential}$, the maximal PAR when atmospheric gases and aerosols are minimal) proposed by Gitelson et al. (2012), as both replace site-based measures of PAR_{TOC} to estimate GPP based on solely remote sensing data and reduce the uncertainties associated with high frequency fluctuations of PAR_{TOC} that result in noise and which do not affect plant photosynthesis (Gitelson et al., 2012; Peng et al., 2013). It should be noted that the computation of $PAR_{potential}$ requires long term PAR_{TOC} measurements for calibration purposes (Gitelson et al., 2012; Peng et al., 2013), being modelled using 6S (Second Simulation of a Satellite Signal in the Solar Spectrum) radiative transfer code (Kotchenova & Vermote, 2007; Vermote et al., 1997), or modelled from a look-up table method (Lyapustin, 2003). In contrast, the computation of PAR_{TOA} only requires several readily available variables such as date and latitude, thereby eliminating the need for long-term PAR_{TOC} measurements or use of more complicated algorithms, thus the modified G-R model facilitates the extension from flux tower to regional scales.

2.6. Ecosystem light-use-efficiency model

Traditional LUE models require separate estimation of fAPAR and ε to compute GPP. However, the coupling of EVI × PAR_{TOC} (Eq. (9)) for estimating GPP implies that EVI can be more explicitly used as a measure of ecosystem light-use-efficiency (eLUE), defined as the ratio between GPP and PAR_{TOC}:

$$eLUE_{TOC} = \frac{GPP}{PAR_{TOC}} = f(EVI) \tag{12}$$

where $eLUE_{TOC}$ (g C MJ^{-1}) was computed for each site using 8-d average GPP (g C m^{-2} d^{-1}) and 8-d average PAR_{TOC} (MJ m^{-2} d^{-1}); f(EVI) was obtained through the regression of $eLUE_{TOC}$ against EVI. Once the $eLUE_{TOC}$ was estimated, an eLUE model for predicting GPP driven by PAR_{TOC} was formulated as:

$$GPP = eLUE_{TOC} \times PAR_{TOC} \tag{13}$$

Similarly, the eLUE can also be defined as the ratio between GPP and PAR_{TOA}:

$$eLUE_{TOA} = \frac{GPP}{PAR_{TOA}} = f(EVI) \tag{14}$$

where $eLUE_{TOA}$ (g C MJ^{-1}) was computed for each site using 8-d average GPP (g C m^{-2} d^{-1}) and 8-d average PAR_{TOA} (MJ m^{-2} d^{-1}); f(EVI) was obtained through the regression of $eLUE_{TOA}$ against EVI. Once $eLUE_{TOA}$ was estimated, an eLUE model for predicting GPP driven by PAR_{TOA} can be formulated as:

$$GPP = eLUE_{TOA} \times PAR_{TOA} \tag{15}$$

To establish the relationship between eLUE and EVI (i.e., to calibrate the eLUE model) and provide independent validation, the dataset from all four NATT sites (354 samples) were first randomized and then divided equally into two subsets, namely calibration dataset (177 samples) and validation dataset (177 samples) respectively. The GPP_{MOD17} dataset was also divided into calibration and validation subsets only for comparison with the other three EVI-based GPP models.

2.7. Data analysis and statistics

Due to data gaps in satellite observations and EC tower measurements, an immediate comparison of the correlations between satellite indices/products and GPP_{EC} may result in biased conclusions due to different subsets of observations. For example, the proportion of 8-day gaps across four NATT sites in LAI_{MOD09}, GPP_{MOD17}, EVI_{MOD09} and GPP_{EC} were 22%, 16%, 12% and 21% respectively. To achieve a more valid comparison of the performances of satellite indices in tracking seasonal variations in GPP_{EC}, we removed tower observations corresponding to satellite index or PAR measurements missing for a particular site-date. Thus, comparisons among all satellite indices as well as variations of EVI-based GPP models were based on exactly the same subset of GPP_{EC} measurements across 4 EC flux tower sites (total of 354, 8-day samples).

To assess the performances for up-scaling the tower derived GPP across biological phenophases, the dataset of each site was further divided into two subsets, namely the green-up phase subset and brown-down phase subset. The green-up phase was defined as the period from minimum GPP preceding the growing season to the peak (maximal GPP), and the brown-down phase was defined as the subsequent period from peak to minimum GPP (i.e., following the cessation canopy greening).

We used three tests to compare the predictions of satellite indices/ products to GPP_{EC}. First, the coefficient of determination (R^2) was computed using the ordinary least-squares (OLS) algorithm to measure the variance of GPP_{EC} that is explained by the satellite indices/products. Second, the analysis of covariance (ANCOVA) was used to test the significance of the differences in linear regression slope and intercept between regression models. Third, we calculated the root mean squared error (RMSE) between measured and modelled GPP values to assess the model accuracy:

$$RMSE = \sqrt{\frac{\sum_{t=1}^{n}(Obs - Pred)^2}{n}} \tag{16}$$

where Obs is the tower measured GPP, $Pred$ is the satellite estimated GPP.

We computed the coefficient of variation (CV) for quantifying the inter-annual variations in GPP. The CV can be computed as:

$$CV = \frac{\sigma}{|\mu|} \times 100 \tag{17}$$

where σ is standard deviation of annual GPP (g C m^{-2} yr^{-1}), $|\mu|$ is the absolute value of the mean annual GPP (g C m^{-2} yr^{-1}).

In this analysis, partial correlation analysis was applied to assess the degree of association between independent and dependent variables while controlling for the effect of another independent variable. Data processing, statistical analysis and visualization were performed in R scientific computation environment (version 3.0.2, R Core Team, 2013) and associated packages contributed by user community (http://cran.r-project.org).

3. Results

3.1. Seasonal and inter-annual variations in meteorology and GPP_{EC}

The seasonal and inter-annual dynamics in EC tower derived GPP (GPP_{EC}) and meteorological variables at four NATT flux tower sites are shown in Fig. 2. Rainfall was highly seasonal with distinct wet and dry seasons (Fig. 2). The intra-annual distribution of rainfall was more random at the southern, xeric site (Ti Tree), resulting in a rainfall pulse-driven vegetation growth patterns (Fig. 2D). Air temperature at these tropical savanna sites was generally above 10 °C year round (Fig. 2). Seasonal peak values in GPP_{EC} decreased from more than 9.25 g C m^{-2} d^{-1} at the most northern, humid Eucalypt woodland site (Howard Springs) to 4.89 g C m^{-2} d^{-1} at the most southern, xeric *Acacia* woodland site (Ti Tree) (Fig. 2). Overall, GPP_{EC} followed rainfall most closely with GPP_{EC} larger in the wet season than dry season (Fig. 2).

3.2. Comparison of satellite products and models in tracking tower GPP

The scatter plots between MODIS vegetation products and GPP_{EC} for each of the four NATT flux tower sites are shown in Fig. 3. $fAPAR_{MOD15}$

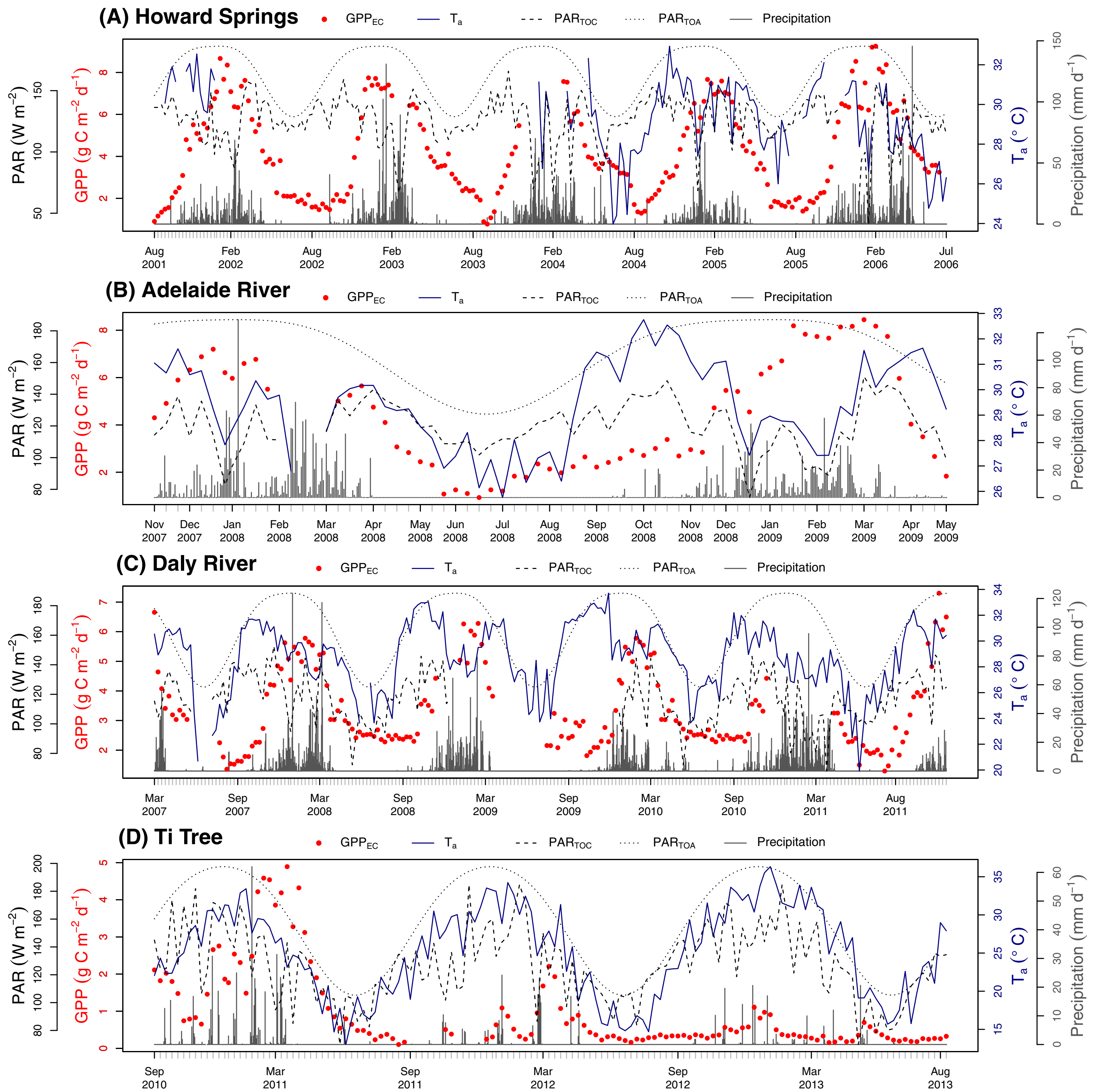

Fig. 2. Seasonal dynamics and inter-annual variations of EC tower derived 8-day averaged GPP (GPP$_{EC}$, g C m^{-2} d^{-1}), photosynthetically active radiation at top-of-canopy (PAR$_{TOC}$, W m^{-2}) and at top-of-atmosphere (PAR$_{TOA}$, W m^{-2}), air temperature (Ta, °C), and daily precipitation (mm d^{-1}) at four flux tower sites. (A) Howard Springs (Eucalypt woodland); (B) Adelaide River (Eucalypt woodland); (C) Daly River (Eucalypt woodland); (D) Ti Tree (*Acacia* woodland).

and GPP$_{MOD17}$ were only moderately correlated with GPP$_{EC}$, with R^2 values of GPP$_{MOD17}$ less than 0.40 at three of the four sites (Fig. 3B–C; Table 2). Overall, NDVI$_{MOD09}$ relationships with GPP$_{EC}$ were equivalent to or a slight improvement to those of fPAR$_{MOD15}$ (Fig. 3D, Table 2). In contrast, LAI$_{MOD15}$ and EVI$_{MOD09}$ were much more strongly correlated with GPP$_{EC}$, with R^2 values between 0.60 and 0.90 (Fig. 3A, E; Table 2). EVI$_{MOD09}$ was slightly more stable with R^2 larger than 0.66 across all individual sites (Fig. 3E; Table 2).

A cross-site analysis showed that NDVI$_{MOD09}$, fAPAR$_{MOD15}$ and GPP$_{MOD17}$ could explain 77% ($F_{1,\,352} = 1197$, $p < 0.0001$), 72% ($F_{1,\,352} = 919.8$, $p < 0.0001$) and 58% ($F_{1,\,352} = 491.2$, $p < 0.0001$) of seasonal variations in GPP$_{EC}$, respectively (Fig. 4B–D; Table 2). In comparison, LAI$_{MOD15}$ and EVI$_{MOD09}$ explained 80% ($F_{1,\,352} = 1412$, $p < 0.0001$) and 84% ($F_{1,\,352} = 1871$, $p < 0.0001$) of seasonal variations in GPP$_{EC}$, respectively (Fig. 4A, E; Table 2). Overall, the EVI$_{MOD09}$ and LAI$_{MOD15}$ products were the best satellite measures for both individual-site and cross-site estimations of GPP$_{EC}$, thus for regional scaling along the NATT study area, we continued our analysis using the slightly better performing EVI$_{MOD09}$.

The coupling of EVI with LST$_{scaled}$ in the T-G model resulted in no improvement in correlations with GPP$_{EC}$ compared to only EVI$_{MOD09}$ at all sites (cf. Figs. 3E and 5A). In contrast, coupling of EVI with PAR$_{TOC}$ in the G-R model improved correlations at Adelaide River ($R^2 = 0.86$, $F_{1,\,41} = 245$, $p < 0.0001$) and Ti Tree sites ($R^2 = 0.79$, $F_{1,\,85} = 317.2$, $p < 0.0001$) (cf. Figs. 3E and 5B) relative to EVI$_{MOD09}$ alone. The coupling of EVI with

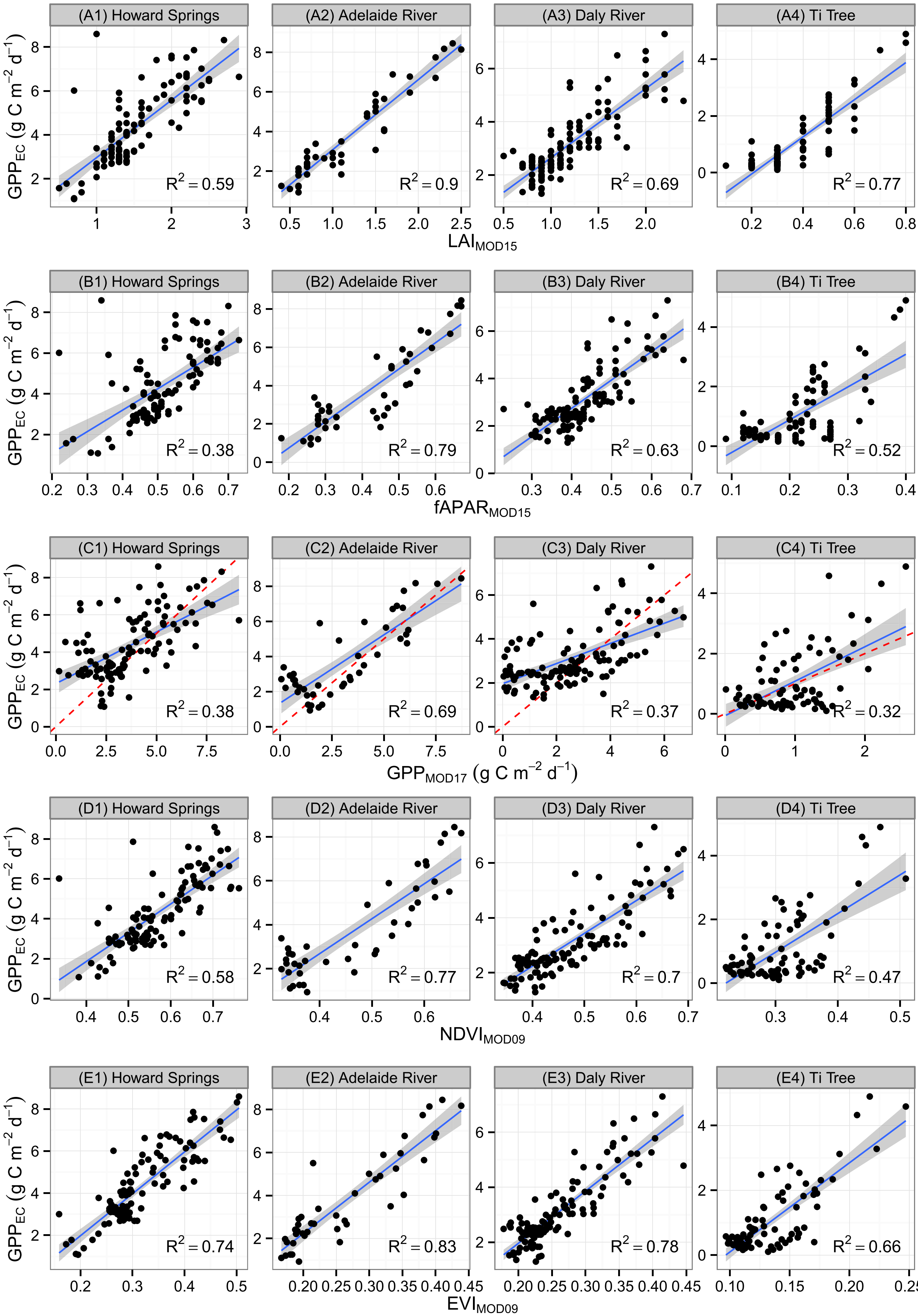
(A1) Howard Springs
(A2) Adelaide River
(A3) Daly River
(A4) Ti Tree
$R^2 = 0.59$
$R^2 = 0.9$
$R^2 = 0.69$
$R^2 = 0.77$
LAI_{MOD15}
(B1) Howard Springs
(B2) Adelaide River
(B3) Daly River
(B4) Ti Tree
$R^2 = 0.38$
$R^2 = 0.79$
$R^2 = 0.63$
$R^2 = 0.52$
$fAPAR_{MOD15}$
(C1) Howard Springs
(C2) Adelaide River
(C3) Daly River
(C4) Ti Tree
$R^2 = 0.38$
$R^2 = 0.69$
$R^2 = 0.37$
$R^2 = 0.32$
GPP_{MOD17} (g C m^{-2} d^{-1})
(D1) Howard Springs
(D2) Adelaide River
(D3) Daly River
(D4) Ti Tree
$R^2 = 0.58$
$R^2 = 0.77$
$R^2 = 0.7$
$R^2 = 0.47$
$NDVI_{MOD09}$
(E1) Howard Springs
(E2) Adelaide River
(E3) Daly River
(E4) Ti Tree
$R^2 = 0.74$
$R^2 = 0.83$
$R^2 = 0.78$
$R^2 = 0.66$
EVI_{MOD09}
GPP_{EC} (g C m^{-2} d^{-1})

Table 2
Summary of the coefficients of determination (R^2) between EC tower derived GPP *versus* MOD15A2 LAI/fAPAR, MOD09A1 NDVI/EVI, MOD17A2 GPP and the products of EVI and scaled-LST, tower measured PAR (PAR_{TOC}), and top-of-atmosphere PAR (PAR_{TOA}) at four NATT sites. The highest R^2 for each site or for cross-sites was highlighted in bold.

Predictor	Cross-sites	Howard Springs	Adelaide River	Daly River	Ti Tree
LAI_{MOD15}	0.80	0.59	**0.90**	0.69	0.77
$fAPAR_{MOD15}$	0.72	0.38	0.79	0.63	0.52
GPP_{MOD17}	0.58	0.38	0.69	0.37	0.32
$NDVI_{MOD09}$	0.77	0.58	0.77	0.70	0.47
EVI_{MOD09}	0.84	0.74	0.83	0.78	0.66
EVI × LST_{scaled}	0.81	0.70	0.78	0.69	0.65
EVI × PAR_{TOC}	0.85	0.69	0.86	0.75	0.79
EVI × PAR_{TOA}	**0.87**	**0.78**	0.89	**0.80**	**0.80**

PAR_{TOA} resulted in further improvements at all sites, with R^2 values ranging between 0.78 and 0.89 over the different savanna vegetation classes and climatic conditions (cf. Figs. 3E and 5C).

In the cross-site analyses, the T-G model decreased the R^2 to 0.81 ($F_{1,\,352} = 1482$, $p < 0.0001$) compared with EVI_{MOD09} alone (cf. Figs. 4E and 6A), while the G-R models improved the R^2 to 0.85 ($F_{1,\,352} = 1964$, $p < 0.0001$) and 0.87 ($R^2 = 0.87$, $F_{1,\,352} = 2276$, $p < 0.0001$) for PAR_{TOC} and PAR_{TOA} respectively (cf. Figs. 4E and 6B, C).

3.3. Disentangling the confounding effect of rainfall and soil moisture content on the relationships between GPP and PAR_{TOA}

We found that coupling EVI_{MOD09} and PAR_{TOA} provided the best model of GPP_{EC} prediction across all NATT sites. However, PAR_{TOA} was also positively correlated with rainfall ($R = 0.42$, $p < 0.001$) and soil water content (SWC) ($R = 0.40$, $p < 0.001$) across all four sites. Since rainfall and SWC, which are primary environmental drivers of savanna photosynthesis, were both positively correlated with GPP_{EC} ($R = 0.52$ and 0.69 respectively, $p < 0.001$), PAR_{TOA} may be providing surrogate information on rainfall and SWC seasonality. To disentangle the confounding effect of rainfall and SWC and to determine whether incorporation of PAR_{TOA} can provide independent and additive predictive ability for predicting GPP_{EC} relative to rainfall and SWC, we conducted a partial correlation analysis to assess the degree of association between PAR_{TOA} and GPP_{EC}, while controlling the effect of rainfall and SWC. Results showed that when the effect of rainfall was held constant, PAR_{TOA} and GPP_{EC} remained significantly correlated ($R = 0.40$, $p < 0.001$), although the correlation was weaker than the simple correlation between PAR_{TOA} and GPP_{EC} ($R = 0.54$, $p < 0.001$).

We also found that SWC alone could explain 48% of the variance in seasonal GPP_{EC} variation across all four NATT sites ($p < 0.001$), while adding PAR_{TOA} increased R^2 to 0.57 ($p < 0.001$). Partial correlation analysis showed that when the effect of SWC was held constant, PAR_{TOA} and GPP_{EC} were still significantly and positively correlated ($R = 0.40$, $p < 0.001$). These results show that PAR_{TOA} provides independent and additive information for predicting savanna GPP_{EC} relative to rainfall and SWC across the four NATT sites.

Finally, we ran an analysis to assess the predictive power of multiple regression models for predicting GPP_{EC} using EVI, PAR_{TOA} and SWC across the NATT sites (Table 3). The model using only EVI_{MOD09} has the highest uncertainty ($R^2 = 0.84$, $p < 0.0001$, RMSE = 0.82 g C m^{-2} d^{-1}), while adding SWC increased model performance ($R^2 = 0.87$, $p < 0.0001$, RMSE = 0.76 g C m^{-2} d^{-1}), and with further incorporation of PAR_{TOA} provided the best GPP_{EC} predictive power ($R^2 = 0.88$, $p < 0.0001$, RMSE = 0.74 g C m^{-2} d^{-1}) (Table 3). Because EVI_{MOD09} already expressed a part of the information of SWC (correlation coefficient between EVI_{MOD09} and SWC was 0.56, $p < 0.0001$), and to keep our model based entirely remote sensing data, we decided not to include SWC into our regional GPP model.

3.4. eLUE models for up-scaling tower GPP

We examined the use of EVI_{MOD09} as a measure of eLUE (defined as GPP/PAR) and analyzed the direct relationships between eLUE and EVI_{MOD09} using PAR_{TOC} ($eLUE_{TOC}$) and PAR_{TOA} ($eLUE_{TOA}$). Fig. 7 presents the cross-site relationships between eLUE and EVI_{MOD09} for calibration and validation datasets, respectively. The regression coefficients and predictive errors are summarized in Table 4. Overall, EVI_{MOD09} correlated strongly with both $eLUE_{TOC}$ ($R^2 = 0.84$, $F_{1,\,175} = 902.7$, $p < 0.0001$, RMSE = 0.0733 g C m^{-2} MJ^{-1}) and $eLUE_{TOA}$ ($R^2 = 0.81$, $F_{1,\,175} = 1003$, $p < 0.0001$, RMSE = 0.0534 g C m^{-2} MJ^{-1}) in the calibration dataset (Fig. 7, Table 4). Likewise in the validation dataset, EVI_{MOD09} showed a strong correlation with $eLUE_{TOC}$ ($R^2 = 0.84$, $F_{1,\,175} = 894.3$, $p < 0.0001$, RMSE = 0.0753 g C m^{-2} MJ^{-1}) and $eLUE_{TOA}$ ($R^2 = 0.85$, $F_{1,\,175} = 1003$, $p < 0.0001$, RMSE = 0.0500 g C m^{-2} MJ^{-1}) (Fig. 7, Table 4), suggesting that spatial and seasonal variations in eLUE can be captured by EVI_{MOD09} across the four NATT sites.

The cross-site linear regression model for calculation of $eLUE_{TOC}$ using EVI_{MOD09} was obtained from the calibration dataset as:

$$eLUE_{TOC} = 1.78 \times (EVI_{MOD09} - d) \tag{18}$$

where d (0.08) is an offset to subtract the contribution of soil background and adjust EVI_{MOD09} to zero when GPP is 0 g C m^{-2} d^{-1} as estimated through inversion of the cross-site GPP_{EC} ~ EVI_{MOD09} linear regression model. The cross-site linear regression model for calculation of $eLUE_{TOA}$ using EVI_{MOD09} was similarly obtained from the calibration dataset as:

$$eLUE_{TOA} = 1.17 \times (EVI_{MOD09} - d) + 0.03 \tag{19}$$

Consequently, a model for calculating GPP using $eLUE_{TOC}$ and PAR_{TOC} was constructed in the sense of the eLUE concept as:

$$GPP = \overbrace{[1.78 \times EVI_{MOD09} - 0.08]}^{eLUE_{TOC}} \times PAR_{TOC} \tag{20}$$

Similarly, a model for calculating GPP using $eLUE_{TOA}$ and PAR_{TOA} was constructed as:

$$GPP = \overbrace{[1.17 \times (EVI_{MOD09} - 0.08)] + 0.03]}^{eLUE_{TOA}} \times PAR_{TOA} \tag{21}$$

Eqs. (20) and (21) represent two models of savanna landscape GPP that use either PAR_{TOC} or PAR_{TOA} in combination with EVI_{MOD09} parameterized eLUE as model input. Hereafter we will refer Eqs. (20) and (21) as $eLUE_{TOC}$ and $eLUE_{TOA}$ models, respectively.

Fig. 8 presents the cross-site relationships between GPP_{EC} and GPP predicted from the eLUE models for the calibration and validation datasets. For comparison, we also present the GPP_{MOD17} and GPP simulated from the EVI_{MOD09} alone (GPP_{EVI}). The model for calculating GPP_{EVI}, i.e., $GPP_{EVI} = (EVI_{MOD09} - 0.08) \times 18.6$, was derived from the linear regression between GPP_{EC} and EVI_{MOD09} using the calibration dataset.

Overall, the $eLUE_{TOC}$ and $eLUE_{TOA}$ models demonstrated better performance in predicting GPP_{EC} than GPP_{MOD17} or GPP_{EVI} (Fig. 8; Table 5). In the validation dataset, the R^2 between GPP_{EC} and GPP predicted using the $eLUE_{TOC}$ model ($GPP_{eLUE\text{-}TOC}$) was 0.85 ($F_{1,\,175} = 1017$, $p < 0.0001$, RMSE = 0.76 g C m^{-2} d^{-1}) (Fig. 8C; Table 5). The correlation between GPP_{EC} and GPP predicted using the $eLUE_{TOA}$ model ($GPP_{eLUE\text{-}TOA}$) was stronger than with the $eLUE_{TOC}$ model ($R^2 = 0.88$, $F_{1,\,175} = 1297$,

Fig. 3. Individual site relationships between satellite indices and EC tower GPP at 8-d time scales. (A) MOD15A2 LAI (LAI_{MOD15}); (B) MOD15A2 fAPAR ($fAPAR_{MOD15}$); (C) MOD17A2 GPP (GPP_{MOD17}); (D) MOD09A1 NDVI ($NDVI_{MOD09}$); (E) MOD09A1 EVI (EVI_{MOD09}). The red dashed line on panel (C) is the 1:1 symmetric line. The blue solid line is the regression line with 95% confidence intervals (grey shaded area).

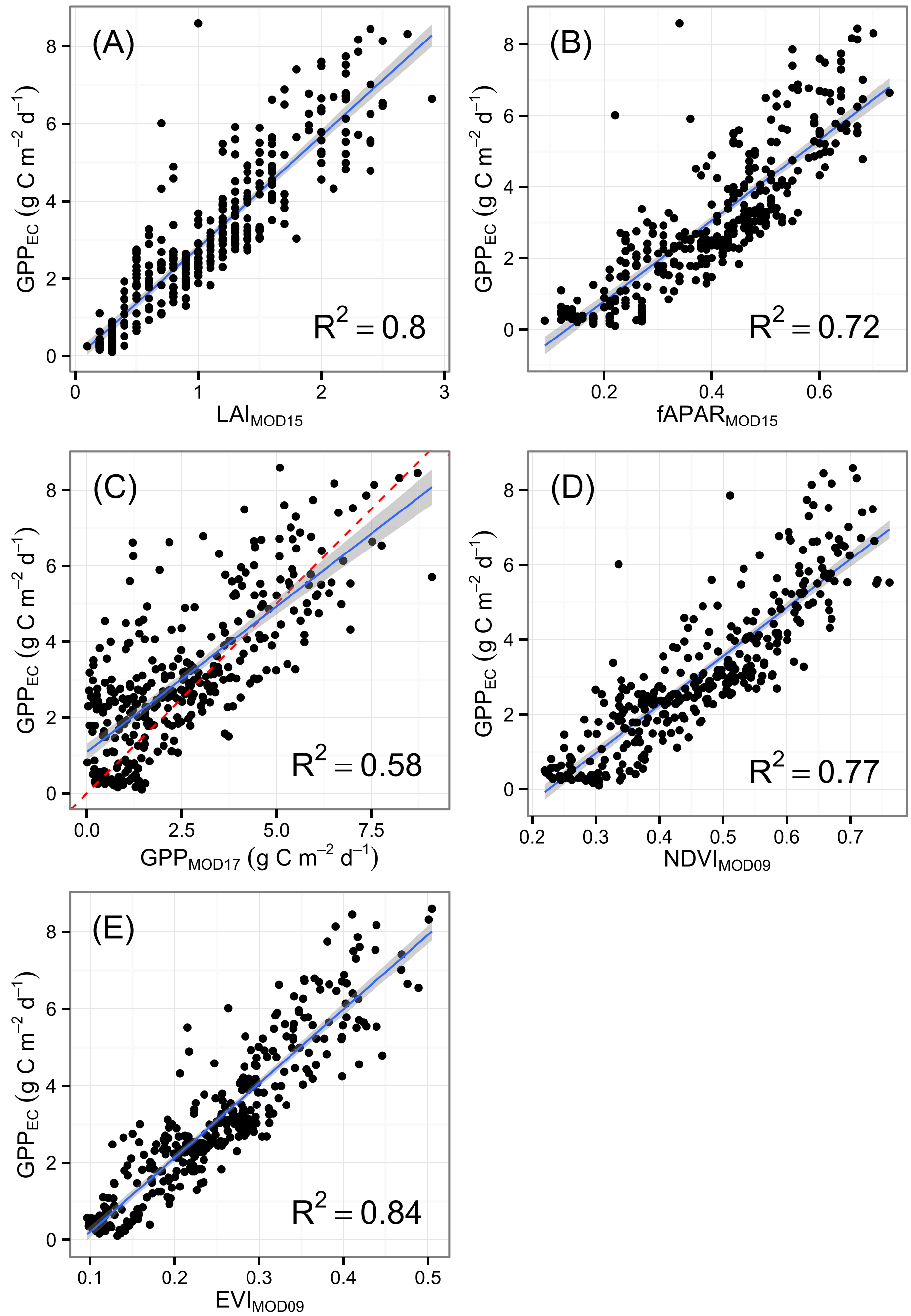

Fig. 4. Cross-site comparisons of satellite indices and EC tower measured GPP across four NATT sites. (A) MOD15A2 LAI (LAI_{MOD15}); (B) MOD15A2 fAPAR ($fAPAR_{MOD15}$); (C) MOD17A2 GPP (GPP_{MOD17}); (D) MOD09A1 NDVI ($NDVI_{MOD09}$); (E) MOD09A1 EVI (EVI_{MOD09}). All $p < 0.0001$. All satellite indices are 8-d temporal resolution. The blue solid line is the regression line with 95% confidence intervals (grey shaded area).

$p < 0.0001$, RMSE $= 0.70$ g C m^{-2} d^{-1}) (Fig. 8D; Table 5). The GPP model based on EVI_{MOD09} alone also performed well for the validation dataset ($R^2 = 0.85$, $F_{1,175} = 978.6$, $p < 0.0001$, RMSE $= 0.78$ g C m^{-2} d^{-1}), suggesting that EVI_{MOD09}, as a measure of eLUE, can explain a large proportion of variations in GPP_{EC} (Fig. 8B; Table 5). In contrast, the predictive power of GPP_{MOD17} to GPP_{EC} was weak and with lower accuracy ($R^2 = 0.58$, $F_{1,\ 175} = 240$, $p < 0.0001$, RMSE $= 1.43$ g C m^{-2} d^{-1}; Fig. 8A; Table 5).

Fig. 9 presents a comparison of time series among satellite and tower derived GPP ($GPP_{eLUE\text{-}TOC}$, $GPP_{eLUE\text{-}TOA}$, GPP_{MOD17} and GPP_{EC}) at the four flux tower sites. Both $GPP_{eLUE\text{-}TOC}$ and $GPP_{eLUE\text{-}TOA}$ matched the seasonal progression of GPP_{EC} quite well (Fig. 9). At the Howard Springs and Daly River sites (*Eucalyptus* woodlands), $GPP_{eLUE\text{-}TOA}$ overestimated GPP_{EC} during the dry season in some, but not all years (Fig. 9A-C). GPP_{MOD17} tended to underestimate productivity during the late dry season to early wet season, except in the *Acacia* woodland (Ti Tree) where underestimation occurred during the wet season (Fig. 9). The *Acacia* woodland was also distinct among the NATT sites with GPP_{eLUE} and GPP_{MOD17} failing to capture the largest and smallest values of GPP_{EC} (Fig. 9E).

3.5. Extension of tower GPP across biologic phenophases

Fig. 10 presents the site-level relationships between satellite derived GPP and GPP_{EC} during green-up and brown-down phenophases across the four NATT sites. Phenophase stage showed distinct relationships between satellite derived GPP and GPP_{EC} at the different NATT sites (Fig. 10). At Howard Springs, the slope of the $GPP_{EC} \sim GPP_{MOD17}$

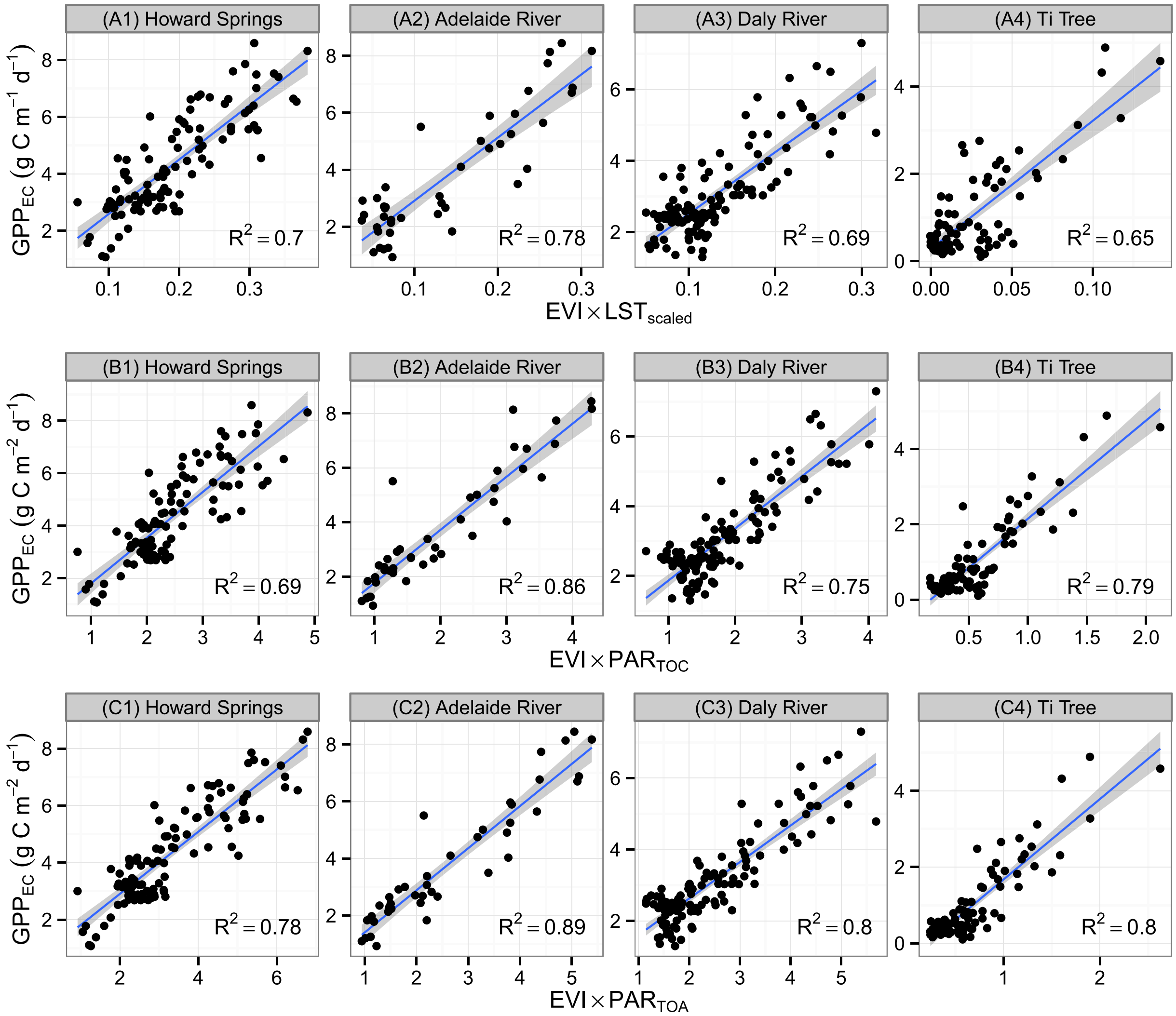

Fig. 5. Site-level relationships between EC tower measured GPP and products of EVI with satellite derived or tower measured meteorological variables. The blue solid line is the regression line with 95% confidence intervals (grey shaded area). LST_{scaled} is scaled MODIS daytime land surface temperature (MOD11). PAR_{TOC} and PAR_{TOA} are PAR incident at top-of-canopy and top-of-atmosphere respectively.

relationship during the green-up phase was not significantly different ($F_{1,\ 103}$ =0.296, $p = 0.588$) from the slope during the brown-down phase; however, there was a very strong offset bias from the 1:1 symmetry line, in which the intercept of the green-up relationships (3.20) was significantly larger ($F_{1,\ 103} = 64.04$, $p < 0.001$) than the intercept of the relationship during brown-down (1.29) (Fig. 10A). At Daly River, the intercept during green-up (2.47) was also significantly larger ($F_{1,\ 115} = 8.13$, $p < 0.001$) than in brown-down (1.48), although the slope was not significantly different between phenophases ($F_{1,\ 115} = 2.54$, $p = 0.114$) (Fig. 10A). At Adelaide River, the green-up slope was significantly smaller than the brown-down slope ($F_{1,\ 40} = 4.54$, $p = 0.040$) (Fig. 10A), while the difference between phenophase responses (i.e., the slope of the GPP_{EC} ~ GPP_{MOD17} relationship) was most pronounced at the Ti Tree site ($F_{1,\ 85} = 18.92$, $p < 0.001$) (Fig. 10A).

Phenophase-dependent bias was reduced in the GPP_{EC} ~ GPP_{EVI} relationships, but remained significant at Howard Springs ($F_{1,\ 103} = 7.42$, $p = 0.008$), Daly River ($F_{1,\ 115} = 8.08$, $p = 0.005$), and Ti Tree ($F_{1,\ 85} = 5.03$, $p = 0.024$), while phenophase slopes were not significantly different at Adelaide River ($F_{1,\ 40} = 2.52$, $p = 0.121$) (Fig. 10B).

Phenophase differences were reduced further, but not removed altogether, by use of the eLUE models (Fig. 10C, D). In the GPP_{EC} ~ $GPP_{eLUE\text{-}TOC}$ relationships, phenophase-dependent slopes were not significantly different at Adelaide River ($F_{1,\ 40} = 0.73$, $p = 0.400$) and Ti Tree ($F_{1,\ 85} = 0.75$, $p = 0.389$), but differences in slope remained at Howard Springs ($F_{1,\ 103} = 10.27$, $p = 0.002$) and Daly River ($F_{1,\ 115} = 14.91$, $p < .001$) (Fig. 10C). In the GPP_{EC} ~ $GPP_{eLUE\text{-}TOA}$ relationships, the phenophase slopes were significantly different at Daly River ($F_{1,\ 115} = 6.30$, $p = 0.005$) and Howard Springs ($F_{1,\ 103} = 4.94$, $p = 0.029$) sites, while only marginally significant at Adelaide River ($F_{1,\ 40} = 4.14$, $p = 0.049$) and Ti Tree ($F_{1,\ 85} = 3.57$, $p = 0.069$) sites (Fig. 10D).

3.6. Biogeographic patterns of savanna GPP over the NATT study area

Fig. 11 illustrates the strong precipitation controls on the spatial and temporal biogeographic patterns of savanna GPP simulated using the $eLUE_{TOA}$ model (Eq. (21)) over the NATT study area. Mean annual GPP decreased from 1400 g C m^{-2} yr^{-1} to less than 400 g C m^{-2} yr^{-1} from the northern humid region to southern xeric region (Fig. 11A). Associated with decreasing mean annual GPP, inter-annual variation in GPP, quantified as the coefficient of variation (CV) of GPP, was generally less than 10% over most northern humid forests and woodlands but increased to more than 30% over the southern xeric grassland and *Acacia* woodland (Fig. 11B).

Fig. 11 also shows a comparison of biogeographic patterns of savanna GPP between wet (January–March) and dry (July–September)

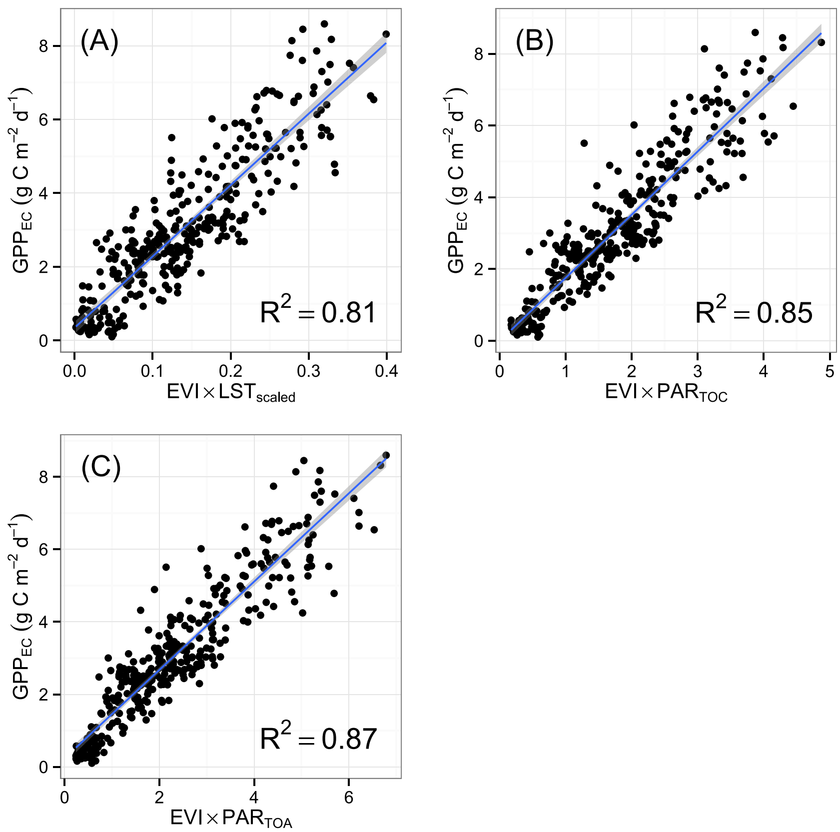

Fig. 6. Cross-site comparisons of scaled temperature and radiation products of EVI and EC tower measured GPP (GPP_{EC}) across four NATT sites. All $p < 0.0001$. All satellite indices are 8-d temporal resolution. The blue solid line is the regression line with 95% confidence intervals (grey shaded area). LST_{scaled} is scaled MODIS daytime land surface temperature (MOD11). PAR_{TOC} and PAR_{TOA} are PAR incident at top-of-canopy and top-of-atmosphere respectively.

seasons. From north to south, the mean daily GPP during the wet season decreased by 66% from more than 6 g C m^{-2} d^{-1} in the coastal, humid region dominated by *Eucalyptus* forests and woodlands to less than 2 g C m^{-2} d^{-1} over the southern, xeric areas, where hummock grasslands and *Acacia* woodlands and shrublands were the dominant vegetation types (Fig. 11C). However, during the dry season, GPP was small with little spatial variability across the NATT (Fig. 11D). Region-wide mean daily GPP during the wet season (2.94 ± 1.44 g C m^{-2} d^{-1}) was almost 2 times larger than the mean daily GPP in the dry season (1.48 ± 0.61 g C m^{-2} d^{-1}), reflecting the large impacts of seasonal rainfall distribution on savanna GPP.

4. Discussion

4.1. Tracking EC tower derived GPP with satellite observations

We found that among five satellite vegetation products, EVI correlated best to EC flux tower derived GPP (GPP_{EC}) across the four mesic-to-xeric NATT sites ($R^2 = 0.84$; Fig. 4E). This was further improved by coupling EVI with PAR_{TOC} ($R^2 = 0.85$; Fig. 6B) or PAR_{TOA} ($R^2 = 0.87$; Fig. 6C), enabling EVI to be used as a measure of eLUE (GPP/PAR). Two savanna landscape eLUE models parameterized with EVI and driven by PAR_{TOC} or PAR_{TOA}, were further analyzed (the $eLUE_{TOC}$ and $eLUE_{TOA}$ models, respectively) for estimation of GPP. The eLUE models resulted in improved GPP predictions across the mesic and xeric savanna sites, suggesting that region-wide GPP can be predicted with reasonable accuracy from entirely satellite remote sensing observations without dependence on interpolated ground meteorology.

We found that GPP_{MOD17} was only moderately correlated with GPP_{EC} ($R^2 = 0.58$; Fig. 4C). All other satellite products (except $fAPAR_{MOD15}$ at Howard Springs) showed much better performances than GPP_{MOD17} in tracking GPP_{EC}. As $fAPAR_{MOD15}$ was better correlated to GPP_{EC} than GPP_{MOD17} (cf. Fig. 3B and C), the introduction of meteorological inputs into GPP_{MOD17} degraded the correlation between GPP_{MOD17} and GPP_{EC}, demonstrating some of the difficulties in accurate estimations of LUE at landscape scales (Kanniah et al., 2009; Sjöström et al., 2013).

Coupling EVI with temperature and radiation measures showed mixed results in predicting savanna GPP. There were no improvements in using the Temperature-Greenness (T-G) model ($EVI_{scaled} \times LST_{scaled}$) for predicting GPP compared with using EVI alone over the NATT study area (cf. Figs. 3E and 5A). This may be due to temperature not being a limiting factor or significant driver of photosynthesis in tropical savannas (Cleverly et al., 2013; Kanniah et al., 2009; Leuning, Cleugh, Zegelin, & Hughes, 2005), or that LST_{scaled} was not an appropriate surrogate measure for radiation. In contrast, we found significant improvements when the Greenness-Radiation (G-R) models (EVI × PAR) were used for predicting GPP_{EC} relative to EVI alone (cf. Figs. 3E–5B and C), reflecting the importance of the quantity (absorbed) of radiation as a critical driver of savanna vegetation productivity (Kanniah, Beringer, & Hutley, 2013a,2013b; Whitley et al., 2011).

Although we didn't find any improvement in GPP estimates using the T-G model over this tropical study area, it is likely that a

Table 3
Results of multiple regression models using EVI_{MOD09}, PAR_{TOA}, and SWC for predicting GPP_{EC} across four NATT sites. The unit of the RMSE is in g C m^{-2} d^{-1}. *F* is the F-value, *df* is the degrees of freedom, *p* is the p-value.

Models	R^2	*F*	*df*	*p*	RMSE
$GPP_{EC} = f(EVI_{MOD09})$	0.84	1763	1, 332	< 0.0001	0.82
$GPP_{EC} = f(EVI_{MOD09}, SWC)$	0.87	1062	2, 331	< 0.0001	0.76
$GPP_{EC} = f(EVI_{MOD09} \times PAR_{TOA})$	0.86	2155	1, 332	< 0.0001	0.79
$GPP_{EC} = f(EVI_{MOD09} \times PAR_{TOA}, SWC)$	0.88	1242	2, 331	< 0.0001	0.74

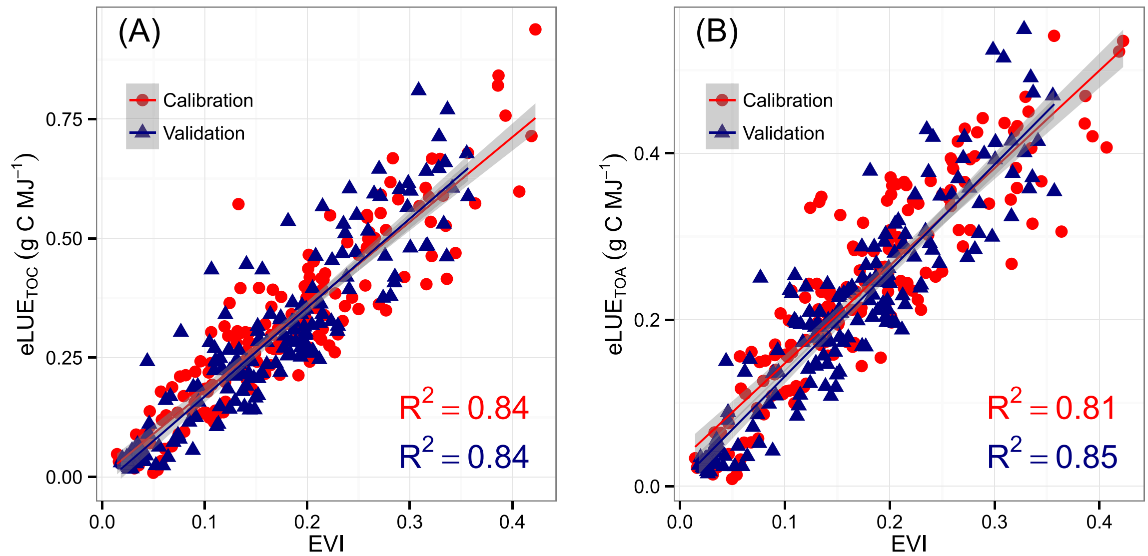

Fig. 7. Cross-site relationships between EVI and eLUE for calibration and validation datasets respectively across four NATT sites. (A) EVI and eLUE$_{TOC}$; (B) EVI and eLUE$_{TOA}$. The blue solid line is the regression line with 95% confidence intervals (grey shaded area). eLUE$_{TOC}$ = GPP$_{EC}$/PAR$_{TOC}$, and eLUE$_{TOA}$ = GPP$_{EC}$/PAR$_{TOA}$. PAR$_{TOC}$ and PAR$_{TOA}$ are PAR incident at top-of-canopy and top-of-atmosphere respectively.

temperature factor would be important in regions where temperature is limiting photosynthesis. In this study, we found that incorporating a temperature scalar (LST), although shown to work well in temperate regions (e.g., Sims et al., 2008; Wu et al., 2012), decreased model performance in this tropical study where vegetation species are well adapted to the warm environment (e.g., C$_4$ grasses dominate the understorey in tropical savannas). Consequently, future studies are needed to develop a generalized framework that can be applied consistently across wider climatic conditions through optimized parameterizations of environmental factors.

We found that coupling EVI with PAR$_{TOA}$ resulted in better predictions of GPP than by coupling EVI with PAR$_{TOC}$ (cf. Fig. 5B and C). This was unexpected as tower measured PAR$_{TOC}$ theoretically should integrate diurnal and seasonal variations in local weather conditions. However, other studies conducted over cropland and grassland flux tower sites have also found that coupling EVI with potential PAR (maximal value of PAR$_{TOC}$) provided better accuracy in predicting GPP than coupling EVI with PAR$_{TOC}$ (Gitelson et al., 2012; Peng et al., 2013; Rossini et al., 2014). Gitelson et al. (2012) attributed the better performance of PAR$_{potential}$ instead of actual PAR$_{TOC}$ to saturation of GPP *versus* PAR$_{TOC}$ at their soybean cropland, noting that a decrease in PAR$_{TOC}$ may not correspond to a decrease in GPP. Over northern Australian savannas, Kanniah et al. (2013a, 2013b) found that the negative effect of decreases in PAR$_{TOC}$ due to wet season cloud cover on rates of photosynthesis were partly compensated by enhanced ε due to the increased proportion of diffuse radiation. Therefore, multiplying EVI by PAR$_{TOA}$ may mimic PAR$_{potential}$ and better approximate radiation controls on GPP.

Table 4
Summary of regression coefficients and RMSE between eLUE and MODIS EVI across four NATT sites, for calibration and validation datasets, respectively. The analysis was based on the 8-d temporal resolution time series. The unit of the RMSE is in g C MJ^{-1}. *F* is the F-value, *df* is the degrees of freedom, *p* is the p-value.

Dataset	eLUE$_{TOC}$ = $\beta_0 + \beta_1 \times$ EVI						
	β_0	β_1	R^2	F	df	p	RMSE
Calibration	0.0000	1.7771	0.84	902.7	1, 175	<0.0001	0.0733
Validation	−0.0176	1.8628	0.84	894.3	1, 175	<0.0001	0.0753
Dataset	eLUE$_{TOA}$ = $\beta_0 + \beta_1 \times$ EVI						
	β_0	β_1	R^2	F	df	p	RMSE
Calibration	0.0303	1.1732	0.81	743	1, 175	<0.0001	0.0534
Validation	0.0046	1.2731	0.85	1003	1, 175	<0.0001	0.0500

4.2. Phenophase impacts on the up-scaling of GPP across seasons

Large discrepancies in the relationship between GPP$_{MOD17}$ and GPP$_{EC}$, and smaller but significant differences in the relationships between GPP$_{EVI}$ and GPP$_{EC}$, were found between green-up and brown-down phenophases at all NATT study sites, particularly at the xeric Ti Tree site (Fig. 10). Phenophase relationships differed in their intercepts and slopes, and they also showed strong nonlinearities during the brown-down phase (Fig. 10). By contrast, the phenophase-dependencies were minimized with the use of eLUE models in the up-scaling of GPP, such that the inclusion of PAR greatly reduced seasonal hysteresis at the Adelaide River and Ti Tree sites (Fig. 10D).

This reduction of phenologic hysteresis in the eLUE model was partly attributed to the differing light conditions encountered between the green-up and brown-down phases. For example, during the green-up at Ti Tree (Nov 2010–Feb 2011), mean PAR$_{TOC}$ and PAR$_{TOA}$ were 12.82 MJ m^{-2} d^{-1} and 16.61 MJ m^{-2} d^{-1} respectively. In contrast, mean PAR$_{TOC}$ and PAR$_{TOA}$ during brown-down (March to July 2011) were 9.11 MJ m^{-2} d^{-1} and 11.11 MJ m^{-2} d^{-1}. This represented a 29% and 33% reduction in PAR$_{TOC}$ and PAR$_{TOA}$, respectively, during the brown-down phase resulting in different radiation environments across phenophases. Therefore, equal values of EVI in green-up and brown-down phases resulted in differing GPP values due to differences in radiation (duration and intensity). Such differences in seasonal light conditions across phenophases were largely normalized in eLUE (GPP/PAR).

The use of eLUE, and in particular PAR$_{TOA}$, may also correct for photoperiod effects on photosynthetic capacity. In a recent study, Bauerle et al. (2012) reported that photoperiod explained more seasonal variation in photosynthetic capacity across 23 tree species than temperature. They also suggested that photoperiod-associated declines in photosynthetic capacity could limit autumn carbon gain in forests, even under favorable autumn conditions (Bauerle et al., 2012). Since photoperiod (day length) is near-linearly correlated with PAR$_{TOA}$ ($R^2 = 0.95$, $F_{1,4352}$, $p < 0.0001$) across the four NATT sites, its incorporation in an eLUE model may potentially correct for photoperiod effects on

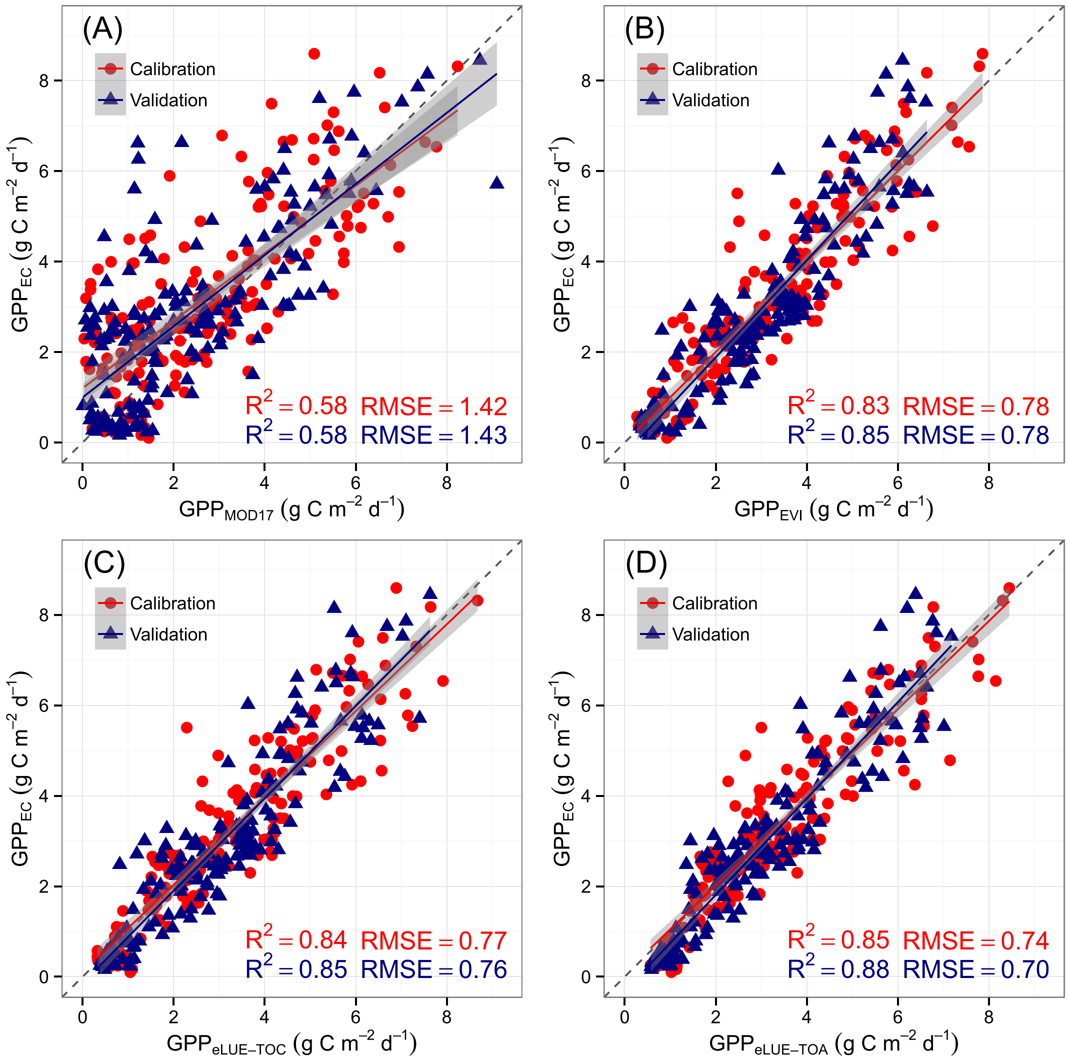

Fig. 8. Cross-site relationships between EC tower derived GPP (GPP_{EC}) and MOD17A2 GPP (GPP_{MOD17}), GPP simulated using EVI alone (GPP_{EVI}), and GPP simulated using eLUE models ($GPP_{eLUE\text{-}TOC}$ and $GPP_{eLUE\text{-}TOA}$). The blue solid line is the regression line with 95% confidence intervals (grey shaded area). The grey dashed line is the 1:1 symmetric line.

photosynthetic capacity. However, further analysis is required to assess the extent to which there is a response of photosynthetic capacity to variations in photoperiod in tropical savannas.

Moisture stress during the brown-down phenophase may also explain some of the residual seasonal hysteresis on the GPP_{EC} ~ $GPP_{eLUE\text{-}TOA}$ relationship. Across the NATT EC flux tower sites, rainfall typically ends in March-April, resulting in the development of large vapor pressure deficits (VPD) and decreased soil moisture content from April through to September (Eamus et al., 2013), coincident with the brown-down phase of GPP at these sites. Whereas declines in GPP_{EC} arise rapidly from stomatal closure during the brown-down phase, chlorophyll degradation and/or the loss of LAI are slower processes that take place at longer time scales (Huemmrich, Privette, Mukelabai, Myneni, & Knyazikhin, 2005; Jenkins et al., 2007; Ma et al., 2013). Future studies are needed to investigate whether the phenophase dependency of GPP could be further reduced by accounting for the rapid declines in photosynthesis associated with stomatal closure.

Despite the differences in green-up and brown-down phase relationships, EVI explained 66% of the variations in GPP_{EC} at the Ti Tree site, while incorporation of PAR_{TOC} and PAR_{TOA} (i.e., the eLUE models) increased the R^2 from 0.66 to 0.79 and 0.80 respectively. This suggested that the eLUE models are able to provide reasonable estimates of GPP at the southern xeric savannas where both species composition and climatic conditions are quite different from the northern mesic savannas.

In addition to the use of an eLUE model, we investigated other ways to adjust the phenophase dependency and found that by fitting separate models for green-up and brown-down, the phenophase impacts can be reduced to the same degree as the site-level eLUE model. For example, EVI_{MOD09} andGPP_{EC} exhibited strong linear relationships during the green-up phase but strong non-linear relationships during the brown-down phase at Ti Tree site (Fig. 10-B4). Thus, by fitting a linear model for green-up phase and a non-linear model (2nd order polynomial) for the brown-down phase, respectively, we found that the hysteresis in the GPP_{EC}~EVI_{MOD09} relationship was well compensated and was better matched to GPP_{EC} than using a single EVI model fitted using data from entire growing season (R^2 increased from 0.69 to 0.86, $p < 0.0001$, RMSE decreased from 0.57 to 0.38 g C m^{-2} d^{-1}). However, the process of separating phenophases and fitting different models is complex and not easily accomplished. In addition, we found that when data from all four sites were pooled together, fitting separate models didn't show improvement as much as using the eLUE model, hence adjusting GPP_{EC}~EVI_{MOD09} hysteresis in this way would be site-dependent. Therefore, the eLUE model provided a simple and consistent way to reduce the phenophase dependency and facilitate an effective extension from flux tower to regional scale.

Table 5
Summary of the regression and error analyses between satellite estimated GPP and EC tower derived GPP across four NATT sites using calibration and validation datasets respectively. The satellite estimated GPP include: MOD17A2 GPP (GPP_{MOD17}), GPP simulated using EVI alone (GPP_{EVI}), GPP simulated by $eLUE_{TOC}$ model (Eq. (20)) ($GPP_{eLUE\text{-}TOC}$), and GPP simulated using $eLUT_{TOA}$ model (Eq. (21)) ($GPP_{eLUE\text{-}TOA}$). The analysis was based on the time series of 8-d temporal resolution. The unit of the RMSE is in g C m^{-2} d^{-1}. *F* is the F-value, *df* is the degree of freedom, *p* is the p-value.

Dataset	$GPP_{EC} = \beta_0 + \beta_1 \times GPP_{MOD17}$						
	β_0	β_1	R^2	F	df	p	RMSE
Calibration	1.2018	0.7454	0.58	240.8	1,175	<0.0001	1.4249
Validation	0.9968	0.7863	0.58	240	1,175	<0.0001	1.4274
Dataset	$GPP_{EC} = \beta_0 + \beta_1 \times GPP_{EVI}$						
	β_0	β_1	R^2	F	Df	p	RMSE
Calibration	0.0000	1.0000	0.83	873.6	1,175	<0.0001	0.7802
Validation	−0.2636	1.0735	0.85	978.6	1,175	<0.0001	0.7766
Dataset	$GPP_{EC} = \beta_0 + \beta_1 \times GPP_{eLUE\text{-}TOC}$						
	β_0	β_1	R^2	F	df	p	RMSE
Calibration	0.1159	0.9593	0.84	924.1	1, 175	<0.0001	0.7659
Validation	−0.1411	1.0208	0.85	1017	1, 175	<0.0001	0.7576
Dataset	$GPP_{EC} = \beta_0 + \beta_1 \times GPP_{eLUE\text{-}TOA}$						
	β_0	β_1	R^2	F	df	p	RMSE
Calibration	0.0771	0.9731	0.85	999.9	1, 175	<0.0001	0.7388
Validation	−0.3198	1.0649	0.88	1297	1, 175	<0.0001	0.6982

4.3. EVI as a measure of ecosystem light-use-efficiency (eLUE)

It was encouraging to see that coupling EVI with the radiation driver, PAR, provided a better estimation of GPP across all study sites. With GPP defined as the product of ε, fAPAR, and PAR (Monteith, 1972), the coupling of EVI with eLUE (or GPP/PAR) translates the EVI, a greenness index, to a function of the product of fAPAR and ε, as:

$$\frac{GPP}{PAR} = eLUE \sim f(EVI) = fAPAR \times \varepsilon \quad (22)$$

Historically, linear relationships between VIs and fAPAR have been well documented through theoretical analyses (Carlson & Ripley, 1997), field measurements (Gamon et al., 1995; Fensholt, Sandholt, & Rasmussen, 2004), and radiative transfer simulations (Carlson & Ripley, 1997; Myneni & Williams, 1994). However, if EVI only represents fAPAR, then one cannot explain the strong relationship between EVI and eLUE, unless (1) the temporal variations in ε are very small, or (2) the temporal variations in fAPAR and ε are synchronized. However, it is well established that ε varies widely across seasons (Jenkins et al., 2007; Sims et al., 2006) and under different types of environmental stress (Ruimy et al., 1995). Furthermore, previous studies have shown that savanna ecosystems in northern Australia utilize radiation more efficiently in the wet season than in the dry season and thus ε exhibits strong seasonality across these sites (Eamus & Cole, 1997; Eamus et al., 2013; Fordyce, Duff, & Eamus, 1995; Kanniah et al., 2009). These studies argue against the first hypothesis that temporal variations in ε are very small, and hence this cannot explain the strong correlation between eLUE and EVI.

The alternative explanation is that the temporal variations in fAPAR and ε are synchronized and hence both are correlated with EVI. In support of this explanation, Sims et al. (2006) reported that ε derived from nine flux towers in North America was strongly correlated to EVI ($R^2 = 0.76$). Similarly, Wu et al. (2012) reported a moderate correlation between EVI and tower ε in temperate and boreal forests of North America. By contrast in evergreen forests, such relationships were weaker than in deciduous forests, or absent in an evergreen oak forest (Goerner, Reichstein, & Rambal, 2009). Thus, we may infer that the correlation between eLUE and EVI was likely due to the synchronization between fAPAR and ε in the ecosystems that the seasonal variations in landscape photosynthesis are primarily driven by dynamics in LAI of deciduous species and/or annual species.

fAPAR (indicated by LAI) and ε in northern Australian savannas exhibit similar phenological patterns (Kanniah et al., 2009; Whitley et al., 2011). In Australian tropical savannas, the primary determinants of seasonal variations in leaf area index, light interception and ecosystem gas exchange are the dynamics of the understorey grasses and forbs, which respond to intra-annual rainfall distribution (Cleverly et al., 2013; Eamus et al., 2013; Hutley, Grady, & Eamus, 2001; O'Grady et al., 2009). In addition, environmental conditions also become favorable for photosynthesis (high soil moisture, low VPD) following the onset of the wet season, thus the ε of both C_3 trees and C_4 grasses is larger in the wet season than the dry season (Eamus, 1999; Eamus & Cole, 1997; Fordyce et al., 1995; O'Grady et al., 2009; Prior, Eamus, & Duff, 1997). Consequently, fAPAR and ε displayed similar phenological patterns in response to changes in environmental factors across north Australian savannas (Kanniah et al., 2009; O'Grady, Chen, Eamus, & Hutley, 2000; Williams, Myers, Muller, Duff, & Eamus, 1997).

In summary, the tight correlation between eLUE and EVI can be attributed to the fact that EVI is not only related to light absorption capacity (fAPAR), but also integrates the effects of phenological stage and environmental stress on photosynthetic efficiency (ε). Although we could derive fAPAR and ε separately, from a remote sensing perspective these ecosystem variables cannot be directly measured by current satellite sensors. Therefore, EVI tends to be a good composite measure that simplifies the up-scaling of carbon fluxes from flux tower to regional scale. The savanna biome consists of multiple plant functional types (PFTs), including differences in fundamental physiology (C_3 *versus* C_4 and nitrogen-fixing *versus* non-fixing) that are difficult to parameterize. Furthermore, the fractions of tree (C_3) and grass (C_4) contributing to ecosystem-scale C fluxes vary across space and time and each PFT has its own unique relationships with environmental factors (Scholes & Archer, 1997). The eLUE model framework presented here represents a substantial improvement to the current MODIS GPP product for tropical savannas, an ecosystem that covers one eighth of the global land area (Scholes & Archer, 1997) and contributes approximately 30% of terrestrial ecosystem GPP (House & Hall, 2001).

5. Conclusions

Measurement of landscape carbon fluxes is an essential task in global change studies, yet current production efficiency models parameterize LUE using coarse resolution, interpolated meteorology, which introduces uncertainties that may reduce the confidence in estimated primary production. In searching for a simple GPP model based entirely on satellite remote sensing observations, we found that MODIS EVI had the strongest cross-site relationships with EC tower derived GPP at both mesic and xeric north Australian savannas. This was further improved by coupling EVI with PAR_{TOC} or PAR_{TOA} and using EVI as a measure of eLUE (GPP/PAR). Two simple savanna landscape GPP models based on eLUEs parameterized using EVI and driven by PAR_{TOC} or PAR_{TOA} were further analyzed, and GPP simulated using these eLUE models agreed well with EC tower derived GPP across all sites. We also found strong biological phenophase dependencies of satellite GPP *versus* tower GPP relationships across green-up and brown-down periods. These dependencies were most pronounced in the MOD17 GPP product, and were considerably reduced by the use of the eLUE models. These results suggest that region-wide savanna GPP can be estimated accurately using entirely satellite remote sensing observations without dependencies on interpolated ground meteorology or estimation of ε.

Approaches in estimating GPP from remote sensing datasets fall into two technical pathways: LUE-based process models and VI-based empirical models. From our analyses, we suggest that replacing LUE (GPP/

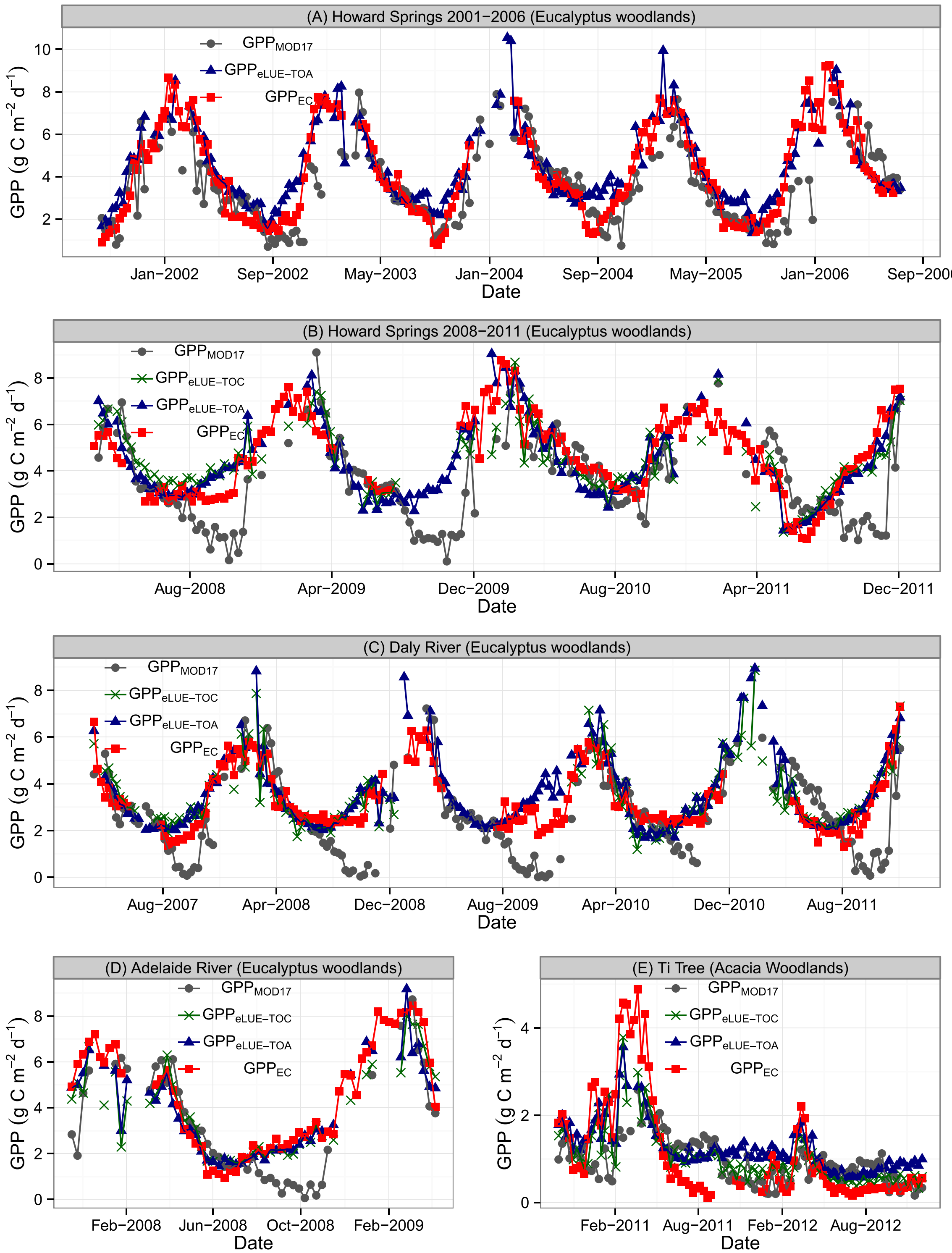

Fig. 9. Time series comparison between MOD17A2 GPP (GPP_{MOD17}), GPP simulated using $eLUE_{TOC}$ model ($GPP_{eLUE-TOC}$, Eq. (20)), simulated using $eLUE_{TOA}$ model ($GPP_{eLUE-TOA}$, Eq. (21)), and EC tower derived GPP (GPP_{EC}) across four NATT sites during 2000–2013. All data are at 8-d temporal resolution.

APAR) with eLUE (GPP/PAR), which is parameterized using readily available MODIS EVI, results in convergence of these two pathways. The convergence yielded simple yet reliable estimates of savanna landscape GPP based entirely on satellite remote sensing observations (through the use of PAR_{TOA}), which has potential to be applied over large scales for better assessment of region-wide savanna carbon dynamics in a truly spatially continuous way.

Acknowledgement

This work was jointly supported by National Basic Research Program of China (No.2012CB955304), Australian Research Council projects ARC-DP140102698, ARC-DP1115479, ARC-DP130101566, and the Chinese Scholarship Council. We appreciate the constructive comments from an anonymous reviewer that helped to improve the paper. We

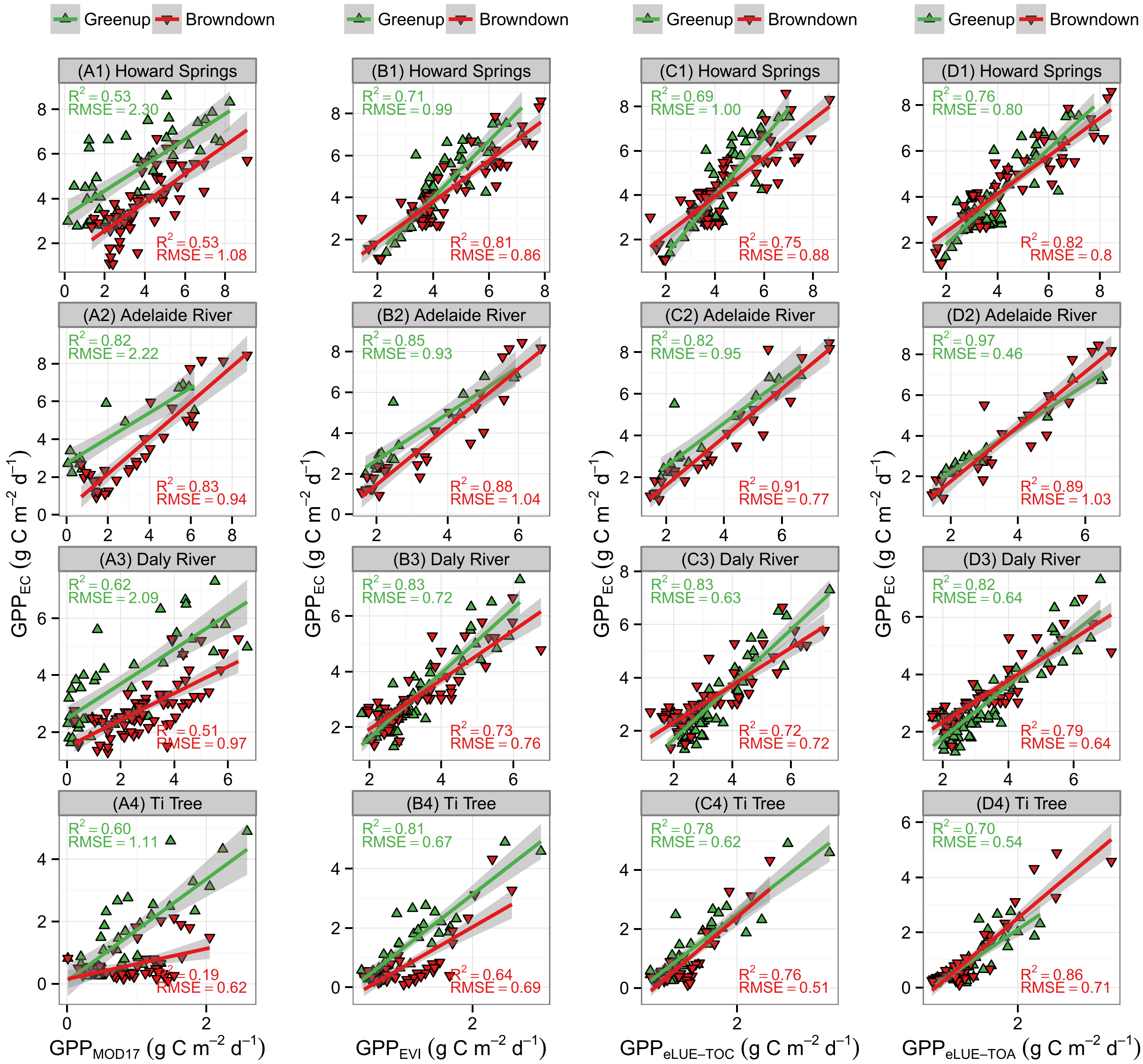

Fig. 10. Site-level relationships between satellite estimated GPP and EC tower derived GPP (GPP_{EC}) for green-up and brown-down phases across four NATT sites. (A1–A4) MODIS GPP product (GPP_{MOD17}); (B1–B4) GPP simulated using EVI alone (GPP_{EVI}); (C1–C4) GPP simulated using $eLUE_{TOC}$ model ($GPP_{eLUE\text{-}TOC}$), and (D1–D4) GPP simulated using $eLUE_{TOA}$ model ($GPP_{eLUE\text{-}TOA}$). The green-up phase is defined as the period from the left trough before greening season to the time of peak GPP, while the brown-down phase is defined as the period following peak GPP to the right trough after the cessation of the greening season. The unit of RMSE is g C m^{-2} d^{-1}.

thank Drs. Kevin Davies and Rakhesh Devadas for maintaining local remote sensing database and for providing e-Research support. We would like to thank all the personnel involved with the operation of the flux towers.

Appendix A. Supplementary data

Supplementary data associated with this article can be found in the online version, http://dx.doi.org/10.1016/j.rse.2014.08.025. These data include Google map of the most important areas described in this article.

References

Baldocchi, D., Falge, E., Gu, L., Olson, R., Hollinger, D., Running, S., et al. (2001). FLUXNET: a New tool to study the temporal and spatial variability of ecosystem-scale carbon dioxide, water vapor, and energy flux densities. *Bulletin of the American Meteorological Society*, *82*(11), 2415.

Bauerle, W. L., Oren, R., Way, D. A., Qian, S. S., Stoy, P. C., THORNTON, P. E., et al. (2012). Photoperiodic regulation of the seasonal pattern of photosynthetic capacity and the implications for carbon cycling. *Proceedings of the National Academy of Sciences*, *109*(22) (201119131-8617).

Beringer, J., Hacker, J., Hutley, L. B., Leuning, R., Arndt, S. K., Amiri, R., et al. (2011). SPECIAL – savanna patterns of energy and carbon integrated across the landscape. *Bulletin of the American Meteorological Society*, *92*(11), 1467.

Carlson, T. N., & Ripley, D. A. (1997). On the relation between NDVI, fractional vegetation cover, and leaf area index. *Remote Sensing of Environment*, *62*(3), 241–252.

Cleverly, J., Boulain, N., Villalobos-Vega, R., Grant, N., Faux, R., Wood, C., et al. (2013). Dynamics of component carbon fluxes in a semi-arid *Acacia* woodland, central Australia. *Journal of Geophysical Research, Biogeosciences*, *118*(3), 1168–1185.

Core Team, R. (2013). *R: A language and environment for statistical computing.* Vienna: Austria R Foundation for Statistical Computing.

Eamus, D. (1999). Ecophysiological traits of deciduous and evergreen woody species in the seasonally dry tropics. *Trends in Ecology & Evolution*, *14*(1), 11–16.

Eamus, D., Cleverly, J., Boulain, N., Grant, N., Faux, R., & Villalobos-Vega, R. (2013). Carbon and water fluxes in an arid-zone *Acacia* savanna woodland: An analyses of seasonal patterns and responses to rainfall events. *Agricultural and Forest Meteorology*, *182–183*(2013), 225–238.

Eamus, D., & Cole, S. (1997). Diurnal and seasonal comparisons of assimilation, phyllode conductance and water potential of three *Acacia* and one *Eucalyptus* species in the wet-dry tropics of Australia. *Australian Journal of Botany*, *45*(2), 275–290.

Fensholt, R., Sandholt, I., & Rasmussen, M. S. (2004). Evaluation of MODIS LAI, fAPAR and the relation between fAPAR and NDVI in a semi-arid environment using in situ measurements. *Remote Sensing of Environment*, *91*(3–4), 490–507.

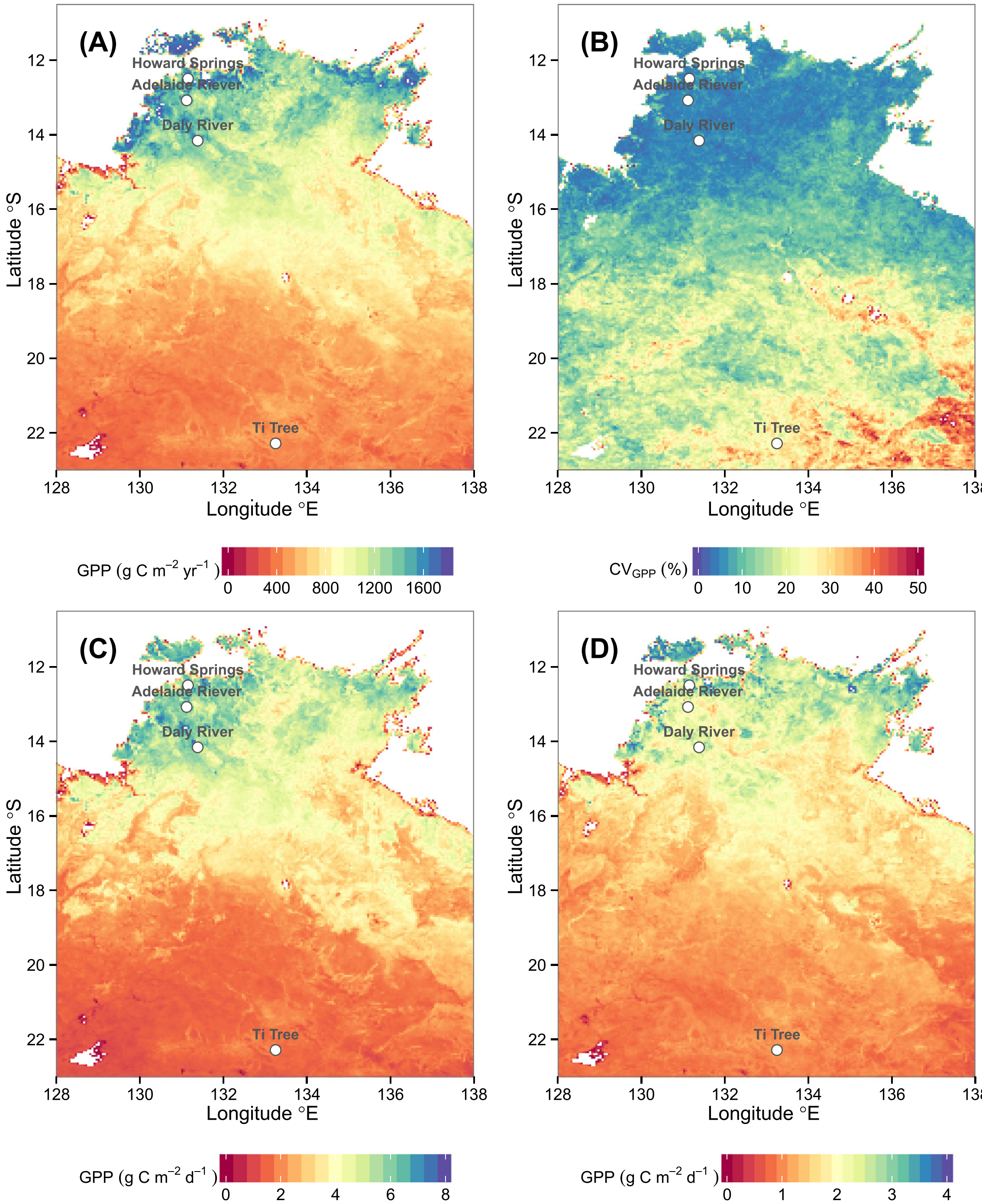

Fig. 11. Biogeographic patterns of GPP over the NATT study area during 2000–2013. (1) Mean annual GPP (g C m^{-2} yr^{-1}); (B) coefficient of variance (CV, %) of annual GPP; (C) Mean daily GPP (g C m^{-2} d^{-1}) during the wet season (January–March); (D) mean daily GPP (g C m^{-2} d^{-1}) during the dry season (July–September). The GPP was simulated using the eLUE$_{TOA}$ model driven by PAR$_{TOA}$ (Eq. (21)).

Fordyce, I. R., Duff, G. A., & Eamus, D. (1995). The Ecophysiology of *Allosyncarpia ternata* (Myrtaceae) in Northern Australia: Tree physiognomy, leaf characteristics and assimilation at contrasting sites. *Australian Journal of Botany*, *43*(4), 367–377.

Gamon, J. A., Field, C. B., Goulden, M. L., Griffin, K. L., Hartley, A. E., Joel, G., et al. (1995). Relationships between NDVI, canopy structure, and photosynthesis in three Californian vegetation types. *Ecological Applications*, *28–41*.

Gitelson, A. A., Peng, Y., Masek, J. G., Rundquist, D. C., Verma, S., Suyker, A., et al. (2012). Remote estimation of crop gross primary production with Landsat data. *Remote Sensing of Environment*, *121*(2012), 404–414.

Gitelson, A. A., Viña, A., Verma, S. B., Rundquist, D. C., Arkebauer, T. J., Keydan, G., et al. (2006). Relationship between gross primary production and chlorophyll content in crops: Implications for the synoptic monitoring of vegetation productivity. *Journal of Geophysical Research*, *111*(D8), D08S11.

Glenn, E. P., Huete, A.R., Nagler, P. L., & Nelson, S. G. (2008). Relationship between remotely-sensed vegetation indices, canopy attributes and plant physiological processes: What vegetation indices can and cannot tell us about the landscape. *Sensors*, *8*(4), 2136–2160.

Goerner, A., Reichstein, M., & Rambal, S. (2009). Tracking seasonal drought effects on ecosystem light use efficiency with satellite-based PRI in a Mediterranean forest. *Remote Sensing of Environment*, *113*(5), 1101–1111.

Gower, S. T., Kucharik, C. J., & Norman, J. M. (1999). Direct and indirect estimation of leaf area index, fAPAR, and net primary production of terrestrial ecosystems. *Remote Sensing of Environment*, *4257*(99), 29–51.

Heinsch, F. A., Zhao, Maosheng, Running, S. W., Kimball, J. S., Nemani, R. R., Davis, K. J., et al. (2006). Evaluation of remote sensing based terrestrial productivity from MODIS using regional tower eddy flux network observations. *IEEE Transactions on Geoscience and Remote Sensing*, *44*(7), 1908–1925.

House, J. I., & Hall, D. O. (2001). Productivity of tropical savannas and grasslands. In H. Mooney, J. Roy, & B. Saugier (Eds.), *Terrestrial global productivity: past, present and future* (pp. 363–400). San Diego, CA: Academic Press.
Huemmrich, K. F., Privette, J. L., Mukelabai, M., Myneni, R. B., & Knyazikhin, Y. (2005). Time–series validation of MODIS land biophysical products in a Kalahari woodland, Africa. *International Journal of Remote Sensing*, *26*(19), 4381–4398.
Huete, A.R., Didan, K., Miura, T., Rodriguez, E. P., Gao, X., & Ferreira, L. G. (2002). Overview of the radiometric and biophysical performance of the MODIS vegetation indices. *Remote Sensing of Environment*, *83*(1–2), 195–213.
Huete, A.R., Didan, K., Shimabukuro, Y. E., Ratana, P., Saleska, S. R., Hutyra, L. R., et al. (2006). Amazon rainforests green-up with sunlight in dry season. *Geophysical Research Letters*, *33*(6), L06405.
Huete, A. R., & Glenn, E. P. (2011). *Remote sensing of ecosystem structure and function. Advances in Environmental Remote Sensing: Sensors, Algorithms, and Applications.* Boca Raton: Taylor and Francis Group, 291–320.
Huete, A.R., Restrepo-Coupe, N., Ratana, P., Didan, K., Saleska, S. R., Ichii, K., et al. (2008). Multiple site tower flux and remote sensing comparisons of tropical forest dynamics in Monsoon Asia. *Agricultural and Forest Meteorology*, *148*(5), 748–760.
Hutley, L. B., Grady, A. P. O., & Eamus, D. (2001). Monsoonal influences on evapotranspiration of savanna vegetation of northern Australia. *Oecologia*, *126*(3), 434–443.
Jenkins, J. P., Richardson, A.D., Braswell, B. H., Ollinger, S. V., Hollinger, D. Y., & Smith, M. L. (2007). Refining light-use efficiency calculations for a deciduous forest canopy using simultaneous tower-based carbon flux and radiometric measurements. *Agricultural and Forest Meteorology*, *143*(1–2), 64–79.
Jin, C., Xiao, X., Merbold, L., Arneth, A., Veenendaal, E., & Kutsch, W. L. (2013). Phenology and gross primary production of two dominant savanna woodland ecosystems in Southern Africa. *Remote Sensing of Environment*, *135*, 189–201.
Jones, D. A., Wang, W., & Fawcett, R. (2009). High-quality spatial climate data-sets for Australia. *Australian Meteorological and Oceanographic Journal*, *58*(4), 233–248.
Kanniah, K. D., Beringer, J., & Hutley, L. B. (2013a). Response of savanna gross primary productivity to interannual variability in rainfall: Results of a remote sensing based light use efficiency model. *Progress in Physical Geography*, *37*(6), 1–22.
Kanniah, K. D., Beringer, J., & Hutley, L. (2013b). Exploring the link between clouds, radiation, and canopy productivity of tropical savannas. *Agricultural and Forest Meteorology*, *182–183*, 304–313.
Kanniah, K. D., Beringer, J., Hutley, L. B., Tapper, N. J., & Zhu, X. (2009). Evaluation of collections 4 and 5 of the MODIS Gross Primary Productivity product and algorithm improvement at a tropical savanna site in northern Australia. *Remote Sensing of Environment*, *113*(9), 1808–1822.
Kergoat, L., Lafont, S., Arneth, A., Le Dantec, V., & Saugier, B. (2008). Nitrogen controls plant canopy light-use efficiency in temperate and boreal ecosystems. *Journal of Geophysical Research*, *113*(G4), G04017.
Koch, G. W., Vitousek, P.M., Steffen, W. L., & Walker, B. H. (1995). Terrestrial transects for global change research. *Vegetatio*, *121*(1–2), 53–65.
Kotchenova, S. Y., & Vermote, E. F. (2007). Validation of a vector version of the 6S radiative transfer code for atmospheric correction of satellite data. Part II. Homogeneous lambertian and anisotropic surfaces. *Applied Optics*, *46*(20), 4455–4464.
Leuning, R., Cleugh, H. A., Zegelin, S. J., & Hughes, D. (2005). Carbon and water fluxes over a temperate Eucalyptus forest and a tropical wet/dry savanna in Australia: measurements and comparison with MODIS remote sensing estimates. *Agricultural and Forest Meteorology*, *129*(3–4), 151–173.
Lyapustin, A. (2003). Interpolation and profile correction (IPC) method for shortwave radiative transfer in spectral intervals of gaseous absorption. *Journal of Atmospheric Science*, *60*, 865–871.
Ma, X., Huete, A., Yu, Q., Coupe, N. R., Davies, K., Broich, M., et al. (2013). Spatial patterns and temporal dynamics in savanna vegetation phenology across the North Australian Tropical Transect. *Remote Sensing of Environment*, *139*, 97–115.
Monteith, J. L. (1972). Solar radiation and productivity in tropical ecosystems. *Journal of Applied Ecology*, *9*(3), 747–766.
Monteith, J., & Unsworth, M. (2013). *Principles of environmental physics – plants, animals, and the atmosphere* (4th ed.). Amsterdam, The Netherlands: Elsevier.
Myneni, R. B., Hoffman, S., Knyazikhin, Y., Privette, J. L., Glassy, J., Tian, Y., et al. (2002). Global products of vegetation leaf area and fraction absorbed PAR from year one of MODIS data. *Remote Sensing of Environment*, *83*(1–2), 214–231.
Myneni, R. B., & Williams, D. L. (1994). On the relationship between FAPAR and NDVI. *Remote Sensing of Environment*, *49*(3), 200–211.
NVIS (2007). *Australia's native vegetation – A summary of Australia's major vegetation groups.*
O'Grady, A. P., Chen, X., Eamus, D., & Hutley, L. B. (2000). Composition, leaf area index and standing biomass of eucalypt open forests near Darwin in the Northern Territory, Australia. *Australian Journal of Botany*, *48*(5), 629–638.
O'Grady, A. P., Cook, P. G., Eamus, D., Duguid, A., Wischusen, J.D. H., Fass, T., & Worldege, D. (2009). Convergence of tree water use within an arid-zone woodland. *Oecologia*, *160*(4), 643–655.
Olofsson, P., Lagergren, F., Lindroth, A., Lindström, J., Klemedtsson, L., Kutsch, W., & Eklundh, L. (2008). Towards operational remote sensing of forest carbon balance across Northern Europe. *Biogeosciences*, *5*(3), 817–832.
Papaioannou, G., Papanikolaou, N., & Retalis, D. (1993). Relationships of photosynthetically active radiation and shortwave irradiance. *Theoretical and Applied Climatology*, *48*(1), 23–27.
Peng, Y., Gitelson, A. A., & Sakamoto, T. (2013). Remote estimation of gross primary productivity in crops using MODIS 250 m data. *Remote Sensing of Environment*, *128*, 186–196.
Prior, L. D., Eamus, D., & Duff, G. A. (1997). Seasonal trends in carbon assimilation, stomatal conductance, pre-dawn leaf water potential and growth in *Terminalia ferdinandiana*, a deciduous tree of Northern Australian savannas. *Australian Journal of Botany*, *45*(1), 53–69.
Rahman, A. F., Sims, D. A., Cordove, V. D., & El-Marsri, B. Z. (2005). Potential of MODIS EVI and surface temperature for directly estimating per-pixel ecosystem C fluxes. *Geophysical Research Letters*, *32*(19), L19404.
Richardson, A.D., & Hollinger, D. Y. (2005). Statistical modeling of ecosystem respiration using eddy covariance data: maximum likelihood parameter estimation, and Monte Carlo simulation of model and parameter uncertainty, applied to three simple models. *Agricultural and Forest Meteorology*, *131*(3), 191–208.
Rossini, M., Migliavacca, M., Galvagno, M., Meroni, M., Cogliati, S., Cremonese, E., et al. (2014). Remote estimation of grassland gross primary production during extreme meteorological seasons. *International Journal of Applied Earth Observations and Geoinformation*, *29*, 1–10.
Rouse, J. W., Jr., Haas, R. H., Schell, J. A., & Deering, D. W. (1973). Monitoring vegetation systems in the Great Plains with ERTS. In S. C. Freden, E. P. Mercanti, & M. Becker (Eds.), *Third Earth Resources Technology Satellite-1 Symposium. Technical presentations, section A, vol. I.* (pp. 309–317). Washington, DC: National Aeronautics and Space Administration (NASA SP-351).
Ruimy, A., Jarvis, P. G., Baldocchi, D.D., & Saugier, B. (1995). CO_2 fluxes over plant canopies and solar radiation: A review. *Advances in Ecological Research*, *26*, 1–68.
Running, S. W., Nemani, R. R., Heinsch, F. A., Zhao, M., Reeves, M., & Hashimoto, H. (2004). A continuous satellite-derived measure of global terrestrial primary production. *BioScience*, *54*(6), 547–560.
Scholes, R. J., & Archer, S. R. (1997). Tree-grass interactions in savannas. *Annual Review of Ecology and Systematics*, *28*(1), 517–544.
Sims, D. A., Luo, H., Hastings, S., Oechel, W. C., Rahman, A. F., & Gamon, J. A. (2006a). Parallel adjustments in vegetation greenness and ecosystem CO_2 exchange in response to drought in a Southern California chaparral ecosystem. *Remote Sensing of Environment*, *103*(3), 289–303.
Sims, D. A., Rahman, A. F., Cordova, V. D., El-Masri, B. Z., Baldocchi, D.D., Bolstad, P. V., et al. (2008). A new model of gross primary productivity for North American ecosystems based solely on the enhanced vegetation index and land surface temperature from MODIS. *Remote Sensing of Environment*, *112*(4), 1633–1646.
Sims, D. A., Rahman, A. F., Cordova, V. D., El-Masri, B. Z., Baldocchi, D.D., Flanagan, L. B., et al. (2006b). On the use of MODIS EVI to assess gross primary productivity of North American ecosystems. *Journal of Geophysical Research*, *111*(G4), G04015.
Sjöström, M., Ardö, J., Arneth, A., Boulain, N., Cappelaere, B., Eklundh, L., et al. (2011). Exploring the potential of MODIS EVI for modeling gross primary production across African ecosystems. *Remote Sensing of Environment*, *115*(4), 1081–1089.
Sjöström, M., Zhao, M., Archibald, S., Arneth, A., Cappelaere, B., Falk, U., et al. (2013). Evaluation of MODIS gross primary productivity for Africa using eddy covariance data. *Remote Sensing of Environment*, *131*, 275–286.
Turner, D. P., Urbanski, S., Bremer, D., Wofsy, S.C., Meyers, T., Gower, S. T., & Gregory, M. (2003). A cross-biome comparison of daily light use efficiency for gross primary production. *Global Change Biology*, *9*(3), 383–395.
Vermote, E. F., Saleous, N. El, Justice, C. O., Kaufman, Y. J., Privette, J. L., Remer, L., et al. (1997). Atmospheric correction of visible to middle-infrared EOS-MODIS data over land surfaces: Background, operational algorithm, and validation. *Journal of Geophysical Research*, *102*, 17131–17141.
Vermote, E. F., Saleous, El, N. Z., & Justice, C. O. (2002). Atmospheric correction of MODIS data in the visible to middle infrared: first results. *Remote Sensing of Environment*, *83*(1–2), 97–111.
Walker, J., & Gillison, A. N. (1982). Australian savannas. In B. J. Huntley, & B. H. Walker (Eds.), *Ecological studies (pp. 5–24)*. Springer Berlin Heidelberg.
Walker, B. H., Steffen, W. L., Canadell, J., & Ingram, J. S. I. (1999). *IGBP Book Series No. 4. The Terrestrial Biosphere and Global Change: Implications for Natural and Managed Ecosystems. Synthesis Volume*Cambridge, UK: Cambridge University Press.
Wan, Z., & Dozier, J. (1996). A generalized split-window algorithm for retrieving land-surface temperature from space. *IEEE Transactions on Geoscience and Remote Sensing*, *34*(4), 892–905.
Whitley, R., Macinnis-NG, C., Hutley, L., Berringer, J., Melanie, Z., Mathew, W., et al. (2011). Is productivity of mesic savannas light limited or water limited? Results of a simulation study. *Global Change Biology*, *17*(10), 3130–3149.
Williams, R. J., Myers, B.A., Muller, W. J., Duff, G. A., & Eamus, D. (1997). Leaf phenology of woody species in a North Australian tropical savanna. *Ecology*, *78*(8), 2542–2558.
Wu, C., Chen, J. M., & Huang, N. (2011). Predicting gross primary production from the enhanced vegetation index and photosynthetically active radiation: Evaluation and calibration. *Remote Sensing of Environment*, *115*(12), 3424–3435.
Wu, C., Chen, J. M., Desai, A. R., Hollinger, D. Y., Arain, M. A., Margolis, H. A., et al. (2012). Remote sensing of canopy light use efficiency in temperate and boreal forests of North America using MODIS imagery. *Remote Sensing of Environment*, *118*, 60–72.
Wu, C., Niu, Z., Tang, Q., Huang, W., Rivard, B., & Feng, J. (2009). Remote estimation of gross primary production in wheat using chlorophyll-related vegetation indices. *Agricultural and Forest Meteorology*, *149*(6–7), 1015–1021.
Wylie, B. K., Johnson, D. A., Laca, E., Saliendra, N. Z., Gilmanov, T. G., Reed, B. C., et al. (2003). Calibration of remotely sensed, coarse resolution NDVI to CO2 fluxes in a sagebrush–steppe ecosystem. *Remote Sensing of Environment*, *85*(2), 243–255.
Xiao, X., Zhang, Q., Hollinger, D., Aber, J., & Moore, B., III (2005). Modeling gross primary production of an evergreen needleleaf forest using MODIS and climate data. *Ecological Applications*, *15*(3), 954–969.
Yuan, W., Liu, S., Yu, G., Bonnefond, J. -M., Chen, J., Davis, K., et al. (2010). Global estimates of evapotranspiration and gross primary production based on MODIS and global meteorology data. *Remote Sensing of Environment*, *114*(7), 1416–1431.
Zhao, M., Heinsch, F. A., Nemani, R. R., & Running, S. W. (2005). Improvements of the MODIS terrestrial gross and net primary production global data set. *Remote Sensing of Environment*, *95*(2), 164–176.